Crossover from directed percolation to mean field behavior in the diffusive contact process

Diploma thesis by
Andreas Messer

Supervised by Prof. Dr. Haye Hinrichsen

Institut für Theoretische Physik und Astrophysik
Julius-Maximilians-Universität, D-97074 Würzburg, Germany

July 8, 2008

Zusammenfassung

In dieser Arbeit haben wir den Kontaktprozess, der von Harris [3] 1974 erstmals beschrieben wurde, um Diffusion erweitert und deren Einfluss auf das Skalenverhalten und das kritische Verhalten untersucht. Der Kontaktprozess ist ein einfaches Model für einen epidemischen Ausbreitungsprozess. Er zeigt einen kontinuierlichen Phasenübergang in einen absorbierenden Zustand. Da die Existenzen eines solchen Zustands die detailierte Balance verletzt, handelt es sich um einen Nicht-Gleichgewichts-Übergang.

Nahe des Phasenübergangs divergieren zeitliche und räumliche Korrelationslängen, was sich im skaleninvarianten Verhalten des Kontaktprozess äußert. So kann ein System durch eine korrekt ausgeführte Reskalierung in ein System anderer Ausdehnung überführt werden. Die damit verbundenen Skalenexponenten zeigen, dass der Kontaktprozess in die Universalitätsklasse der gerichteten Perkolation einzuordnen ist.

In dieser Arbeit untersuchen wir, wie sich Diffusion, die wir als Hüpfprozess zwischen benachbarten Gitterplätzen einführen, auf die Eigenschaften solcher Systeme auswirkt. Von besonderem Interesse ist hier der Einfluss der Diffusionsrate auf die Skalenexponenten und den kritischen Kontrollparameter.

Wir beginnen mit einer Einführung in die Phänomenologie des diffusiven Kontaktprozesses in der wir die drei Skalenexponenten der gerichteten Perkolation definieren. Anschließend zeigen wir, dass eine korrekte Beschreibung des Verhaltens mittels Mean-Field Rechnung nicht möglich ist und motivieren so die Verwendung von Feldtheoretischen Methoden. Im darauf folgenden Kapitel zeigen wir im Detail, wie der diffusive Kontaktprozess mit einer Feldtheorie beschrieben werden kann. Im Zuge der Ein-Schleifen-Korrektur werden der kritische Kontrollparameter berechnet und der Zusammenhang zum Skalenverhalten hergestellt.

Im Anschluss an diese Rechnung präsentieren wir numerische Ergebnisse für die berechneten Größen, die wir mittels Monte Carlo Simulationen ermittelt

haben.

Wir schließen die Arbeit mit einer numerischen Lösung der Ein-Schleifenkorrektur.

Contents

Contents

1. Introduction

Phase transitions are an import field of research in physics. They occur in a wide range of processes in environment and many processes in nature depend on them. Common examples for phase transitions are the melting and vaporising of water, the super conductivity of metals at low temperatures and the transition to paramagnetic behaviour observed in ferromagnetic materials.

Phase transitions can be divided into to two main groups, the first order and the continuous phase transitions. The former are characterised by the existence of latent heat which is released or absorbed at the transition. Melting ice or vaporising water belong into this case. The continuous phase transitions don't show this behaviour. Instead they are characterised by diverging correlation lengths at the transition. This kind of phase transitions can be observed in Ising magnets or the directed percolation model.

As a consequence of the diverging length scales, observables behave as power laws close to the transition. These are characterised by certain critical exponents which often depend on the dimensionality of the system. Therefore systems which show a continuous phase transition are scale invariant under appropriate rescaling of parameters, lengths and times. Wilson [15] discovered that this behaviour can be described by a renormalisation group approach.

Considering the scaling exponents, continuous phase transitions can be classified into several universality classes. Because of its robustness against modifications, the directed percolation universality class plays an important role here.

Directed percolation was introduced as a simple model of a spreading process by Broadbent and Hammersley [1] fifty years ago. For instance it can be interpreted as wetting of a porous material where the wetting media has a preferred direction of flow. In this model the material is represented by a diagonal cubic lattice where each site is connected to adjacent sites with a certain probability. The probability plays the role of the control parameter of the phase transition.

1. Introduction

Depending on its value the media can penetrate infinite deep into the material or the wetting stops at a certain depth. If once all sites of layer are dry, the system is captured in an absorbing state. Therefore directed percolation is a non equilibrium process.

The directed percolation universality class is characterised by the three critical exponents β, $\nu_\parallel$ and $\nu_\perp$ which describe the scaling of the particle density, of the correlation length parallel and perpendicular to the preferred direction of flow.

Another possibility to represent the directed percolation model, is to interpret the preferred direction as a time and wet sites as particles on a cubic lattice. This picture is called the 'contact process'. Here the wetting or not wetting of adjacent site corresponds to creation of particles on empty sites by neighbouring particles and the spontaneous death of particles. In this dynamic description the death of particles occurs with rate 1 and the creation rate λ plays the role of the control parameter.

Based on this model a generalised diffusive contact process can be defined by introducing diffusion of particles. Besides creation and annihilation, particles can hop to neighbouring sites with a rate D in this model. As diffusion enhances the mixing of the lattice one expects that the system crosses over from a directed percolation to a mean field behaviour for increasing diffusion constants.

In a recent work Dantas et al. [2] studied the one dimensional diffusive contact process. They showed that the crossover can be described in terms of a crossover exponent ϕ. Using series expansion and partial differential approximants they found that in one spatial dimension $3 \leq \phi \leq 4$.

In this work (published as [9]) we use a field theoretic approach to verify this result and to extend it to higher spatial dimensions. Furthermore we present results of extensive Monte Carlo simulations in order to confirm our calculations.

We start our analysis with an introduction into the phenomenological properties of the diffusive contact process in chapter 2. After that we show that a mean field description does not give the right results in order to motivate the use of a field theory. We continue with a detailed explanation of the field theoretic treatment in chapter 3. In the last chapter 4 we evaluate the numerical data from Monte Carlo simulations and compare the results with our analytical proposals.

2

2. Mean field analysis

2.1. Phenomenology of the diffusive contact process

The diffusive contact process is a toy model for an epidemic spreading process. It is defined on an infinite large d-dimensional hyper-cubic space lattice. Infected individuals are represented as particles which reside on the sites of this lattice. As on each site only one particle is allowed to reside, the particle density can not exceed one:

$$0 \leq \rho\left(t\right) \leq 1. \tag{2.1}$$

The evolution in time occurs in a random sequential manner which means, that a random lattice site is chosen and if it is occupied one of the three possible moves is performed. Introducing reaction rates, which describe how often such a micro process occurs in a unit time interval per particle, these moves may be defined as follows:

1. An existing particle creates new particles on empty next neighbouring lattice sites with rate λ/d with d being the spatial dimension of the system. For example in one space dimension there are the two possibilities

$$\tag{2.2}$$
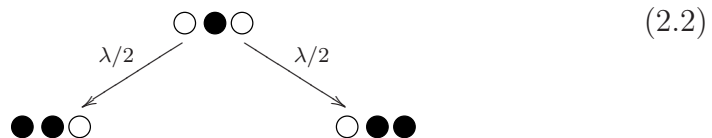
for this reaction.

2. A particle hoops to a random neighbouring site with rate D if this site is

empty. In one space dimension this corresponds to

$$
\begin{array}{c}
\circ\,\bullet\,\circ \\
D/2 \swarrow \qquad \searrow D/2 \\
\bullet\,\circ\,\circ \qquad\qquad \circ\,\circ\,\bullet
\end{array}
\qquad . \qquad (2.3)
$$
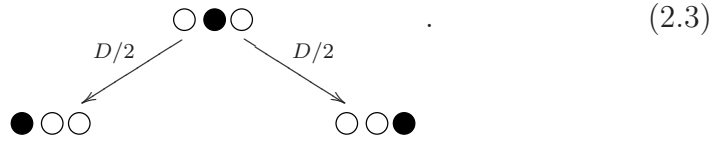
3. A particle dies with rate one.

$$
\begin{array}{c}
\circ\,\bullet\,\circ \\
1 \downarrow \\
\circ\,\circ\,\circ
\end{array}
\qquad (2.4)
$$

In addition to the explicit diffusion micro process, the creation and death of particles cause an intrinsic diffusion. This happens when a particle creates offspring and dies afterwards:

$$
\begin{array}{c}
\circ\,\bullet\,\circ \\
\lambda/2 \swarrow \qquad \searrow \lambda/2 \\
\bullet\,\bullet\,\circ \qquad\qquad \circ\,\bullet\,\bullet \\
1 \downarrow \qquad\qquad\quad 1 \downarrow \\
\bullet\,\circ\,\circ \qquad\qquad \circ\,\circ\,\bullet
\end{array}
\qquad (2.5)
$$
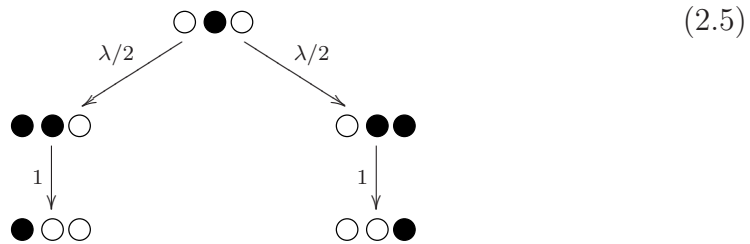
This set of dynamic rules clearly generates an absorbing state which, once entered, can not be left anymore. This state is characterised by an empty lattice and will be reached after a finite time for creation rates λ below the percolation threshold λ_c as shown in figure 2.1. For $\lambda > \lambda_c$ the system stays in the active state and the density of particles becomes a constant after a sufficient amount of time. Close to the phase transition this stationary density behaves as

$$
\rho_{\text{stat}} \sim (\lambda - \lambda_c)^\beta \text{ for } \lambda > \lambda_c \qquad (2.6)
$$

where β is the critical scaling exponent of the particle density.

Another import property of the diffusive contact process and of continuous phase transitions in general is related to the spatial and temporal correlation lengths $\tilde{\xi}_\perp$ and $\tilde{\xi}_\parallel$. They may be defined as follows: In a super-critical system
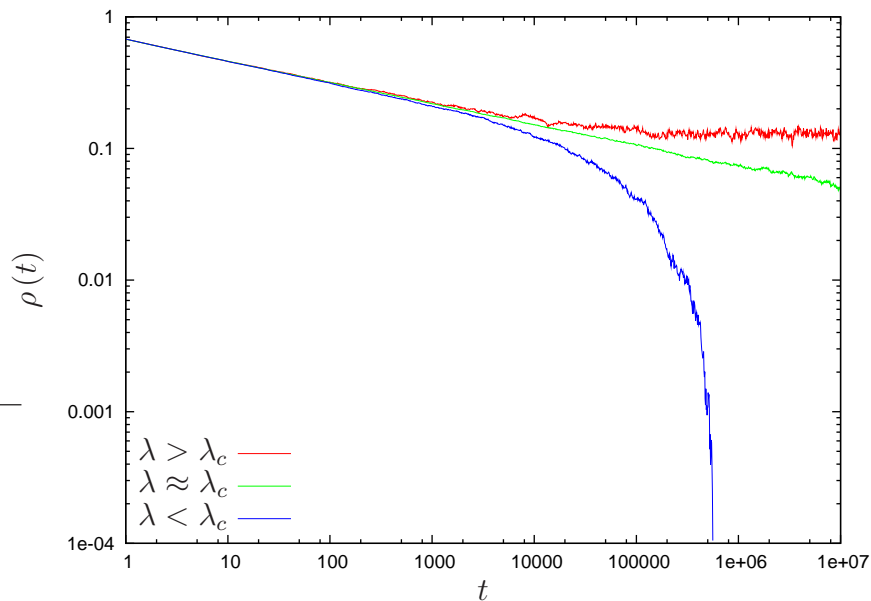
Figure 2.1.: Time evolution of average particle density $\rho(t)$ in dependence of creation rate. The graph shows the saturation for super-critical systems (red line), the power law decay at criticality (green line) and the exponential decay in sub-critical systems (blue line).

the spatial correlation length can be regarded as a measure for the diameter of empty regions and the temporal correlation length is proportional to the time an area stays unoccupied as shown in figure 2.2(a). For sub-critical systems it is more sensible to relate the correlation lengths to the decay time of a cluster and its extend at the origin like in figure 2.2(b).

As systems contain holes and clusters of different sizes it is sensible to study the distribution of these correlation lengths. In figure 2.3 the spatial auto-correlation function of a one dimensional system is shown. This function is proportional to the distribution of spatial correlation length $\tilde{\xi}_\perp$. Away from criticality the distribution decays exponentially for large correlation lengths. Indeed for small correlation lengths a power law behaviour emerges. Because of the exponential decay it is possible to define an average correlation length $\xi_\perp$ respectively. Upon approaching the critical percolation threshold the power law behaviour supersedes the exponential decay. Hence the average correlation length increases until it diverge at criticality. The same holds for the average temporal correlation length $\xi_\parallel$.
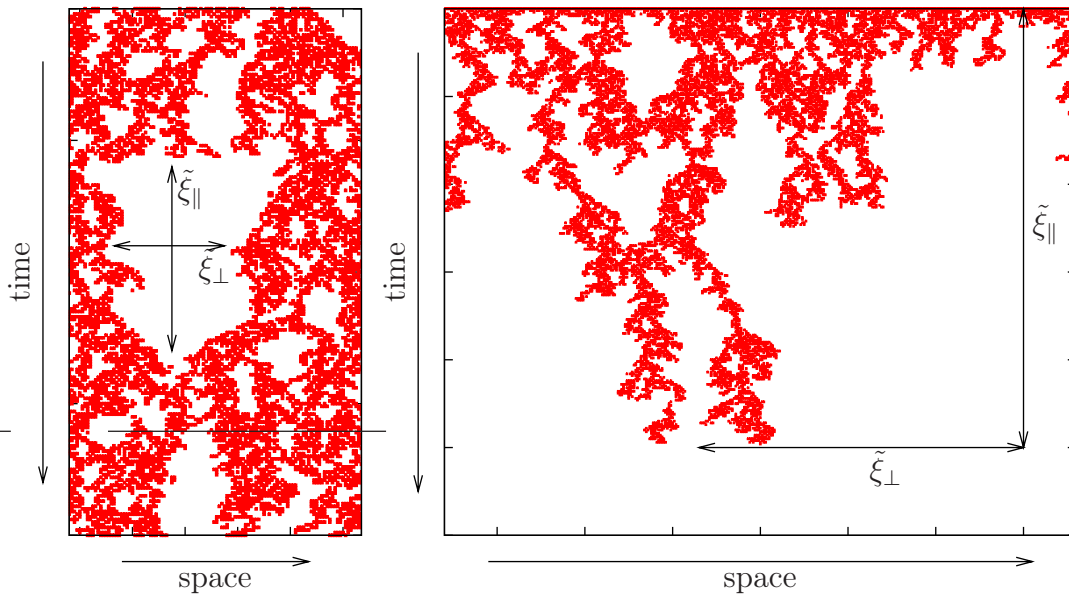
(a) In super-critical systems the extend of the empty regions defines the correlation lengths.

(b) For sub-critical systems the correlation length can defined through the the base line and the height of the active clusters.

Figure 2.2.: The plot shows the time development of a one dimensional diffusive contact process. The graphs depict a cut out of the lattice for a certain time interval.

The behaviour upon approaching the phase transition can be described as

$$\xi_\perp \sim |\lambda - \lambda_c|^{-\nu_\perp}, \quad \xi_\parallel \sim |\lambda - \lambda_c|^{-\nu_\parallel} \tag{2.7}$$

which defines the two scaling exponents $\nu_\perp$ and $\nu_\parallel$. At the phase transition, when $\lambda = \lambda_c$, one also observes a power law behaviour of the density

$$\rho(t) = t^{-\delta}\rho(1) \tag{2.8}$$

where $\delta = \beta/\nu_\parallel$ is a combination of the previously introduced exponents.

By varying the diffusion constant D, the diffusive contact process can be tuned to behave as the ordinary non diffusive contact process ($D = 0$) or to a fully coupled mean field regime ($D \to \infty$) where all sites are mutually coupled. This is called the crossover from directed percolation to diffusive contact process.
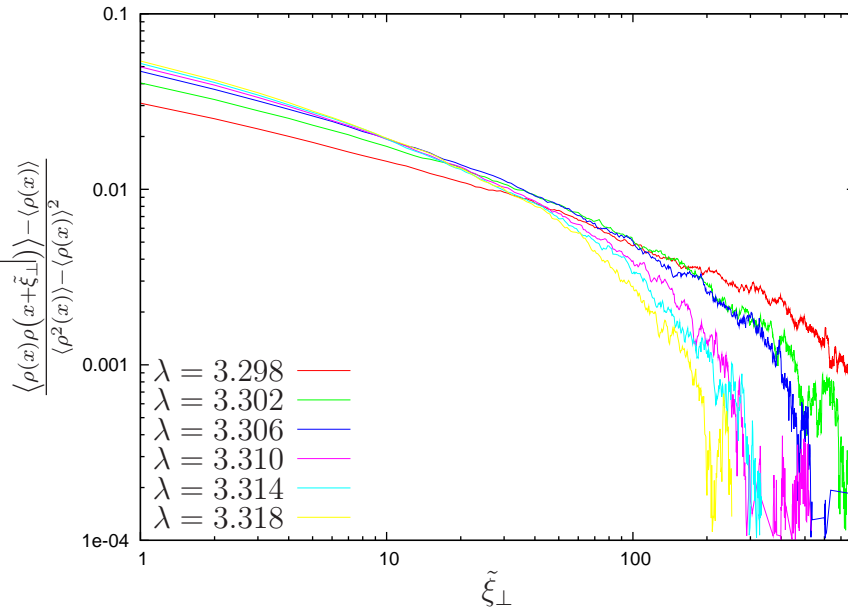
Figure 2.3.: Auto-correlation function of a one dimensional diffusive contact process measured at time-point $t = 100000$. The power law behaviour for short correlation lengths becomes an exponential decay with increasing correlation length $\tilde{\xi}_\perp$. Upon approaching the critical percolation threshold $\lambda_c \approx 3.2979$ the power law part of the distribution widens.(Fixed simulation parameters: diffusion constant $D = 0$)

2.2. Mean field equation

Denoting the probability, that a lattice site at i is occupied at time t by

$$P_t(i)$$

we calculate the occupation probability at time $t + 1$ by considering the dynamical rules described previously. According to these prescription we find the following contributions to $P_{t+1}(i)$:

$P_t(i)$: the probability the site i was occupied at time t,

$\frac{\lambda}{2d} \sum_{j \in NN} (1 - P_t(i)) P_t(j)$: (the sum runs over nearest neighbours) the probability the site i was not occupied at time t but a particle was created by a neighbouring particle at this site.

$\frac{D}{2d} \sum_{j \in NN} (1 - P_t(i)) P_t(j)$: the probability the site i was not occupied at time t but a neighbouring particle diffused to the site it.

7

2. Mean field analysis

$-\frac{D}{2d}\sum_{j\in NN} P_t(i)(1-P_t(j))$: the probability the particle on the site i hopped to a empty neighbouring site.

$-P_t(i)$: the probability the particle died.

Summing over these terms yields the master equation

$$P_{t+1}(i) = \frac{\lambda}{2d}\sum_{j\in NN}(1-P_t(i))P_t(j) + \frac{D}{2d}\sum_{j\in NN}(P_t(j)-P_t(i)) \qquad (2.9)$$

which describes how the probability, that a lattice site i is occupied by a particle at time $t+1$, can be computed from the occupation probabilities at time t. While this relation is an exact description of the system, it is not possible to find a solution to it. Hence it is necessary to find sensible simplifications of this expression. To this end, we concentrate on the regime close to the phase transition. Here, as correlation lengths become large, we can average over an area of lattice sites which is small compared to the correlated regions without destroying the geometric properties. Consequently we define a density of particles

$$\rho_t(x) \approx \langle P_t(i)\rangle_{|x_i-x|\ll\xi_\perp} \qquad (2.10)$$

on a continuous spatial space where the subscript reminds to average over small areas.

Furthermore, taking the random sequential dynamics of the process into account, we know that a move of a single particle corresponds to an advance in time by

$$\Delta t = \frac{1}{(1+\lambda+D)N} \qquad (2.11)$$

with N being the number of lattice sites. With respect to the large number of sites this allows us to replace the discrete time by a quasi-continuous time. Adding the Term $-\rho_t(x)$ to (2.9) and taking the limit $\Delta t \to 0$ we end up with the mean field equation of the diffusive contact process

$$\frac{\partial}{\partial t}\rho(t,x) = \frac{D}{2d}\nabla^2\rho(t,x) + (\lambda-1)\rho(t,x) - \lambda\rho^2(t,x). \qquad (2.12)$$

8

Table 2.1.: Numerical estimates for certain critical exponents of directed percolation compared with the mean field exponents of the diffusive contact process. As we expect diffusion not change these exponents, they can be regarded valid for the diffusive contact process too.

exponent	$d = 1$ [7]	$d = 2$ [14]	$d = 3$[6]	mean field
β	0.2277730(5)	0.584(4)	0.81(1)	1
$\nu_\perp$	1.096854(4)	0.734(4)	0.581(5)	$1/2$
$\nu_\parallel$	1.733847(6)	1.295(6)	1.105(5)	1

2.3. Scaling behaviour

To examine the over critical behaviour of (2.12) we take into account that the average density ρ becomes a constant after a sufficiently long evolution time. We therefore set the derivatives zero and obtain the two stationary solutions

$$\lim_{t \to \infty} \rho(t, x) = \begin{cases} 0 & \text{for } \lambda < 1 \\ \frac{\lambda - 1}{\lambda} & \text{for } \lambda \geq 1 \end{cases} \tag{2.13}$$

for the particle density. The first solutions corresponds to the absorbing and the second one to the active state. From this result we find that

$$\lambda_c = 1, \quad \beta = 1. \tag{2.14}$$

The remaining exponents can be determined using the scale behaviour close to the phase transition. Using relations (2.6), (2.7) and (2.12) we find

$$x \to \Lambda x, \quad t \to \Lambda^{\nu_\parallel / \nu_\perp} t, \quad \Delta \to \Lambda^{-1/\nu_\perp} \Delta, \quad \rho \to \Lambda^{-\beta/\nu_\perp} \rho, \quad D \to D \tag{2.15}$$

for the scaling properties of parameters and density. Here Λ plays the role of an arbitrary dilatation factor. Because of the power law behaviour of the density at the phase transition, the system shall stay invariant under such a rescaling. A simple dimensional analysis of (2.12) then leads to exponents

$$\nu_\perp = \frac{1}{2}, \quad \nu_\parallel = 1. \tag{2.16}$$

A comparison with the results of numerical simulations, presented in table

2. Mean field analysis

2.1, shows quite big differences between the mean field results and the numerical estimates for the exponents. This is related to the fact, that a mean field approach neglects local fluctuations of the order parameter by definition. Unfortunately it turns out, that these fluctuations become important for systems with spatial dimension d below a certain critical dimension d_c. Above this critical dimension the mixing between the sites is large enough to keep the influence of the local fluctuations small. Hence mean field exponents are valid for $d \geq d_c$.

In case of the directed percolation this dimension is four. To calculate exponents below these critical dimension several methods have been developed over the past years whereas the two major ones are series expansion and field theory. While series expansion delivers good estimates for the critical percolation threshold λ_c and the exponents, it is not usable for high dimensional systems due to the increasing complexity (in most cases $d = 1$). In contrast to that, field theory is the appropriate tool to study phase transitions close to the critical dimension. With more effort[1] it is also possible to use field theory far away from the critical dimension.

As we want to study the diffusive contact process in context of different spatial dimension, we will continue with a field theoretic approach in the next chapter.

---

[1]The lower the dimension the higher the necessary order in calculations.

10

3. Field-theoretical approach

In the past years field theoretic methods, that have already been used to describe relativistic quantum scattering processes, exposed to be also a very strong tool to investigate the scaling behaviour of phase transitions of non equilibrium systems. Furthermore, the field theoretic renormalisation procedure provides a nice interpretation of the origin and an explanation of the scale behaviour of a desired system. As this methods are now known for several years, we will avoid a detailed introduction into field theoretic basics here. Instead we will present how to set up a field theory for a a stochastic process. Further and more detailed information may be found in [10, 13, 12].

3.1. Derivation of field theoretic action

The central quantity of a field theoretic description of a certain system is the so called Lagrange density (*Lagrangian*). Integrating this density over space and time gives the action of the system. In order to derive the Lagrangian of a stochastic process, it is common to start from the mean field equation. For the diffusive contact process we had (2.12) which suffers from the following penalty. As a result of the averaging and coarse graining, the mean field model does not respect the stochastic nature of the process. To reintroduce this property we extend equation (2.12) by a noise term $\xi(x,t)$:

$$\frac{\partial}{\partial t}\rho(t,x) = \frac{D}{2d}\Delta\rho(t,x) + (\lambda - 1)\rho(t,x) - \rho^2(t,x) + \xi(x,t). \qquad (3.1)$$

This expression is called a coarse grained Langevin equation [5]. For the diffusive contact process the noise has to fulfil the condition

$$\langle\xi(x,t)\xi(y,t')\rangle = \Gamma\rho(x,t)\,\delta^d(x-y)\,\delta(t-t'). \qquad (3.2)$$

3. Field-theoretical approach

where the dependence on ρ prohibits particle creation in vacuum. This is necessary to ensure the existence of the absorbing state. To reproduce this two point correlator the probability distribution of noise and density must be proportional to the functional

$$P\left[\xi, \rho\right] \sim \exp\left(-\int d^d x dt \frac{\xi^2\left(x, t\right)}{2\Gamma \rho\left(x, t\right)}\right) \tag{3.3}$$

where the value of the functional describes how likely the system can be described by a certain noise and density configuration. The parameter Γ denotes the noise strength.

Unfortunately, a straight forward solution of (3.1) is not possible as both fields depend on each other and both are unknown. A possible solution is not to calculate the fields ρ and ξ in a direct way but considering observables composed of combinations of such fields.

To this end we introduce the concept of an observable. An observable is usually a combination of fields at certain space time points and can be computed as an average of the fields weighted by the probability distribution. For instance we define

$$A\left(x, t, y, t'\right) = \rho\left(x, t\right)\rho\left(y, t'\right) \tag{3.4}$$

we then have for the observable

$$\mathcal{A}\left(x, t, y, t'\right) = \int D\rho \int D\xi \, \rho\left(x, t\right)\rho\left(y, t'\right)P\left[\rho, \xi\right] \tag{3.5}$$

where we have introduced the functional integral $\int D^1$. This expression shows, that not only one configuration (ρ, ξ) of fields is involved in calculating an observable. Indeed all possible solutions contribute with a certain weight given by (3.3).

As this probability would give a non zero contribution for arbitrary fields, it is necessary to extend it by a functional delta function

$$\delta\left[\rho, \xi\right] \sim \int D\tilde{\rho} \exp\left(\imath \int d^d x \, dt \, \tilde{\rho}\left(x, t\right) \cdot f\left(\rho\left(x, t\right), \xi\left(x, t\right)\right)\right) \tag{3.6}$$

to exclude all unwanted field configurations from the averaging process. By

---

[1]see appendix A

choosing

$$f(\rho) = \left(\frac{\partial}{\partial t} - \frac{D}{2d} \nabla^2 - (\lambda - 1) \right) \rho + \lambda \rho^2 - \xi \qquad (3.7)$$

only solutions of (3.1) can contribute. Therefore configurations which do not belong to the phase space of the diffusive contact process are excluded. Collecting all terms we find

$$\mathcal{O}(\cdots) = \int D\xi D\rho D\tilde{\rho} \, O[\cdots] \, P[\rho, \xi] \times$$
$$\exp\left(\imath \int d^d x dt \tilde{\rho} \left(\frac{\partial}{\partial t} - \frac{D}{2d} \nabla^2 - (\lambda - 1) \right) \rho + \lambda \tilde{\rho} \rho^2 - \tilde{\rho} \xi \right). \qquad (3.8)$$

for a generic observable $\mathcal{O}$. Now the noise can be eliminated in favour of the field $\tilde{\rho}$ by Gaussian integration which yields

$$\mathcal{O}(\cdots) = \int D\rho D\tilde{\rho} \, O[\cdots] (\rho, \tilde{\rho}) \times$$
$$\exp\left(\imath \int d^d x dt \tilde{\rho} \left(\frac{\partial}{\partial t} - \frac{D}{2d} \nabla^2 - (\lambda - 1) \right) \rho + \lambda \tilde{\rho} \rho^2 + \imath \frac{\Gamma}{2} \tilde{\rho}^2 \rho \right). \qquad (3.9)$$

As an outcome of this step, the new term $\imath \frac{\Gamma}{2} \tilde{\rho}^2 \rho$ appeared.

This first important result is a path integral similar to the ones found in quantum field theory. Therefore the methods developed over the past years can be applied for further evaluation of this expression.

3.2. Observables in field theory

In the previous section we have introduced the concept of computing an observable as an average over an functional of a set of fields weighted by a probability distribution. During this calculation a new field $\tilde{\rho}$ appeared which turns out to play an important role when computing observables.

If we understand (3.9) as a quantum field theory the fields $\tilde{\rho}$ and ρ may be interpreted as creation and annihilation operators. In this picture, the "measurement" of an observable corresponds to a particular "scattering process" from an initial- into a final state. For instance the two point correlation function

$$C(y - x, t' - t) \sim \langle \rho(y, t') \rho(x, t) \rangle \qquad (3.10)$$

describes the correlation between space time point (y, t') and (x, t). From the view of a scattering process this corresponds to particle creation at (x, t), propagation to (y, t') and annihilation there:

$$\bullet\!\!\longrightarrow\!\!\bullet = \int D\rho \int D\tilde{\rho}\rho\,(y, t')\,\tilde{\rho}\,(x, t) \exp\left(-\int d^d x dt \mathcal{L}\right) \qquad (3.11)$$

where $\mathcal{L}$ denotes the Lagrangian of the system. In case of the particle density

$$\rho\,(t) = \left\langle \frac{1}{V} \int d^d x \rho\,(x, t) \right\rangle, \quad \rho\,(0) = 1 \qquad (3.12)$$

the scattering representation becomes more complicated. It is necessary to respect all possible ways, how a particle could appear at the space time point (x, t). For instance two, three, four and even infinite particle processes have to be regarded:

$$\bullet\!\!\longrightarrow\!\!\bullet\;,\quad \succ\!\!\!\longrightarrow\!\!\bullet\;,\quad \succ\!\!\!\!\succ\!\!\longrightarrow\!\!\bullet \qquad (3.13)$$

Furthermore all all possible initial state space time points have to be taken into account. Expressing this in terms of an exponential we have

$$\rho\,(t) = \frac{1}{V} \int d^d x \int D\rho \int D\tilde{\rho}\rho\,(x, t) \exp\left(\int d^d y dt'\,\tilde{\rho}\,(y, t')\right) \exp\left(-\int d^d y dt \mathcal{L}\right) \qquad (3.14)$$

for the particle density. An important property of this relation is, that on the right hand side the field $\tilde{\rho}$ occurs only within the exponential. Therefore the scaling properties of the observable 'density' are completely determined by the field ρ which is what one would expect.

In a similar way other observables can be expressed in terms of combination of fields (operators) at certain space time points.

3.3. Symmetries

Like in quantum field theory, symmetries of the action lead to restrictions on parameters and fields. For the diffusive contact process, it turns out that the fields ρ and $\tilde{\rho}$ can be related to each other.

From (3.9) we find

$$\mathcal{L} = -\imath\tilde{\rho}\left(\frac{\partial}{\partial t} - \frac{D}{2d}\nabla^2 - (\lambda - 1)\right)\rho - \imath\lambda\tilde{\rho}\rho^2 + \frac{\Gamma}{2}\tilde{\rho}^2\rho \qquad (3.15)$$

for the diffusive contact process. Employing a rescaling and renaming of parameters and fields

$$\rho \quad \rightarrow \quad \phi = \rho\sqrt{\frac{2\lambda}{\imath\Gamma}} \qquad (3.16)$$

$$\tilde{\rho} \quad \rightarrow \quad \tilde{\phi} = -\imath\tilde{\rho}\sqrt{\frac{\imath\Gamma}{2\lambda}} \qquad (3.17)$$

$$\sqrt{\imath\frac{\Gamma\lambda}{2}} \quad \rightarrow \quad g \qquad (3.18)$$

$$\tilde{\phi}\frac{\partial}{\partial t}\phi \quad \rightarrow \quad \frac{1}{2}\left(\tilde{\phi}\frac{\partial}{\partial t}\phi - \phi\frac{\partial}{\partial t}\tilde{\phi}\right) \qquad (3.19)$$

$$\tilde{\phi}\cdot(\lambda - 1)\cdot\phi \quad \rightarrow \quad \tilde{\phi}\kappa\phi. \qquad (3.20)$$

and partial integration of the action, this expression can be rewritten as

$$\mathcal{L} = \frac{1}{2}\left(\tilde{\phi}\frac{\partial}{\partial t}\phi - \phi\frac{\partial}{\partial t}\tilde{\phi}\right) + D\left(\nabla\tilde{\phi}\right)\left(\nabla\phi\right) - \tilde{\phi}\kappa\phi + g\left(\tilde{\phi}\phi^2 - \tilde{\phi}^2\phi\right) \qquad (3.21)$$

and

$$\mathcal{O}(\cdots) = \int D\phi \int D\imath\tilde{\phi}\, O\,[\cdots]\exp\left(-\int d^d x\, dt\, \mathcal{L}\right). \qquad (3.22)$$

In (3.21) the time reversal symmetry of the diffusive contact process can easily be seen. Replacing the fields and time according to

$$\phi(x,t) \rightarrow -\tilde{\phi}(x,-t), \quad \tilde{\phi}(x,t) \rightarrow -\phi(x,-t), \quad -t \rightarrow \tau \qquad (3.23)$$

we re-obtain 3.21. Because of this symmetric behaviour under exchange of fields, both fields ϕ and $\tilde{\phi}$ have the same dimension and scaling properties.

3.4. Generating functional

We have shown in the previous sections, that each observable can be expressed in terms of the fields ϕ and $\tilde{\phi}$ (ρ and $\tilde{\rho}$ respectively). The next step is to derive a functional, from which a desired observable can be calculated. A common

approach to this issue is to set up a generating functional.

Introducing external currents J and $\tilde{J}$ we define this generating functional as[2]

$$Z\left[J, \tilde{J}\right] = \frac{\int D\phi \int D\imath\tilde{\phi}\exp\left(-\int_{xt}\mathcal{L} + \int_{xt}\phi J + \int_{xt}\tilde{\phi}\tilde{J}\right)}{\int D\phi \int D\imath\tilde{\phi}\exp\left(-\int_{xt}\mathcal{L}\right)} \tag{3.24}$$

where the denominator ensures a proper normalisation

$$Z\left[J, \tilde{J}\right]\Big|_{J,\tilde{J}=0} \overset{!}{=} 1 \tag{3.25}$$

of this partition sum. Each desired observable can now calculated by taking the functional variation of (3.24) and setting external currents to zero.

$$O\left(x,t\cdots\right) = \left\langle O\left[\phi, \tilde{\phi}\right](x,t)\cdots\right\rangle = \left(\frac{\delta}{\delta J\left(x,t\right)}\cdots\right)Z\left[J, \tilde{J}\right]\Big|_{J=0,\tilde{J}=0} \tag{3.26}$$

3.5. Solution of generating functional

In order to calculate observables we need to work out a more usable form of (3.24). To this end we split the Lagrangian (3.21) into a free part

$$\mathcal{L}_{free} = \frac{1}{2}\left(\tilde{\phi}\frac{\partial}{\partial t}\phi - \phi\frac{\partial}{\partial t}\tilde{\phi}\right) + \frac{D}{2d}\left(\nabla\tilde{\phi}\right)\left(\nabla\phi\right) - \tilde{\phi}\kappa\phi \tag{3.27}$$

and an interacting part

$$\mathcal{L}_{int} = g\left(\tilde{\phi}\phi^2 - \tilde{\phi}^2\phi\right). \tag{3.28}$$

The free part describes the propagation or movement of a free particle and its life time and therefore contains all terms which are quadratic in the fields. The interacting part accounts for particle creation and the limit on the particle density.

The following calculations are common methods in quantum field theory and are mainly taken from [12].

---

[2] $\int_{xt}$ is short for $\int d^dx\, dt$

3.5.1. Non interacting part

In this section we will focus on finding a solution to the free part of the Lagrangian. We consider the non-interacting generating functional

$$Z_0\left[J, \tilde{J}\right] \sim \int D\phi \int D\imath\tilde{\phi} \exp\left(-\int_{xt} \mathcal{L}_{free} + \int_{xt} \phi J + \int_{xt} \tilde{\phi}\tilde{J}\right) \qquad (3.29)$$

where the normalisation has been omitted. By shifting the fields ϕ and $\tilde{\phi}$ according to

$$\phi \to \phi + \phi_0, \quad \tilde{\phi} \to \tilde{\phi} + \tilde{\phi}_0. \qquad (3.30)$$

and requiring that the new fields ϕ_0 and $\tilde{\phi}_0$ fulfil the differential equations

$$\left(+\frac{\partial}{\partial t} - \frac{D}{2d}\nabla^2 - \kappa\right)\phi_0 = \tilde{J} \qquad (3.31)$$

$$\left(-\frac{\partial}{\partial t} - \frac{D}{2d}\nabla^2 - \kappa\right)\tilde{\phi}_0 = J \qquad (3.32)$$

we separate the externals currents in (3.29) from the functional integral. This yields

$$Z_0\left[J, \tilde{J}\right] \sim \exp\left(\frac{1}{2}\int_{xt}\left(\tilde{\phi}_0\tilde{J} + \phi_0 J\right)\right) \times \int D\phi \int D\tilde{\phi} \exp\left(-\int_{xt}\mathcal{L}\right) \qquad (3.33)$$

where the latter part does not depend on the external currents anymore. It can be integrated and gives a pure number. This number can be absorbed in a global normalisation factor leading to

$$Z_0\left[J, \tilde{J}\right] \sim \exp\left(\frac{1}{2}\int_{xt}\left(\tilde{\phi}_0\tilde{J} + \phi_0 J\right)\right). \qquad (3.34)$$

To find a solution for (3.31) and (3.32) we set

$$\phi_0(x, t) = \int d^d y dt' \tilde{J}(y, t') \bar{\Delta}_F(x - y, t - t') \qquad (3.35)$$

$$\tilde{\phi}_0(x, t) = \int d^d y dt' \bar{\Delta}_F(y - x, t' - t) J(y, t') \qquad (3.36)$$

where the $\bar{\Delta}_F(x, t)$ is called the propagator of the system. This function can

3. Field-theoretical approach

be expressed in terms of a Fourier integral as

$$\bar{\Delta}_F (x, t) = \int d^d k d\omega \frac{e^{\iota(kx+\omega t)}}{(2\pi)^{d+1}} \frac{1}{\frac{D}{2d}k^2 - \kappa + \iota\omega}. \qquad (3.37)$$

Inserting (3.35) and (3.36) into (3.34) yields

$$Z_0 \left[J, \tilde{J} \right] \sim \exp\left(\int d^d x dt \int d^d y dt' \tilde{J}(x, t) \bar{\Delta}_F (y - x, t' - t) J(y, t') \right) \qquad (3.38)$$

which reads in momentum space representation

$$Z_0 \left[J, \tilde{J} \right] \sim \exp\left(\int d^d k d\omega \tilde{J}(-k, -\omega) \Delta_F (k, \omega) J(k, \omega) \right) \qquad (3.39)$$

where
$$\Delta_F (k, \omega) = \frac{1}{\frac{D}{2d}k^2 - \kappa + \iota\omega}. \qquad (3.40)$$

As already pointed out, the free Lagrangian describes the propagation and life time of a single particle. Regarding our definition of the two point correlation function (3.11) we find

$$C(y - x, t' - t) = \left. \frac{\delta}{\delta J(y, t')} \frac{\delta}{\delta \tilde{J}(x, t)} Z_0 \left[J, \tilde{J} \right] \right|_{J, \tilde{J}=0} = \bar{\Delta}_F (y - x, t' - t)$$

$$(3.41)$$

for a free particle. As this corresponds to particle creation at (x, t) and particle annihilation at (y, t') the propagator is the probability that a particle diffuses the distance $y' - x$ in time $\Delta t = t' - t$. As the propagator depends on differences only, the 2-point correlation function is translational invariant.

Another important property of the propagator is, that it clearly obeys causality. This can be seen upon applying the residue theorem to the time integral in (3.37). For $\Delta t > 0$, when particle annihilation occurs after creation, the integration path lies in the upper half of the complex ω-plane as shown in figure 3.1(a). Instead for $\Delta t < 0$ the curve has to be closed in the lower half (figure 3.1(b)). According to the position of the pole we find that only momenta with

$$|k| > \kappa \frac{2d}{D} \text{ for } \Delta t > 0 \qquad (3.42)$$

$$|k| < \kappa \frac{2d}{D} \text{ for } \Delta t < 0 \qquad (3.43)$$

(a) $\Delta t > 0$ (b) $\Delta t < 0$
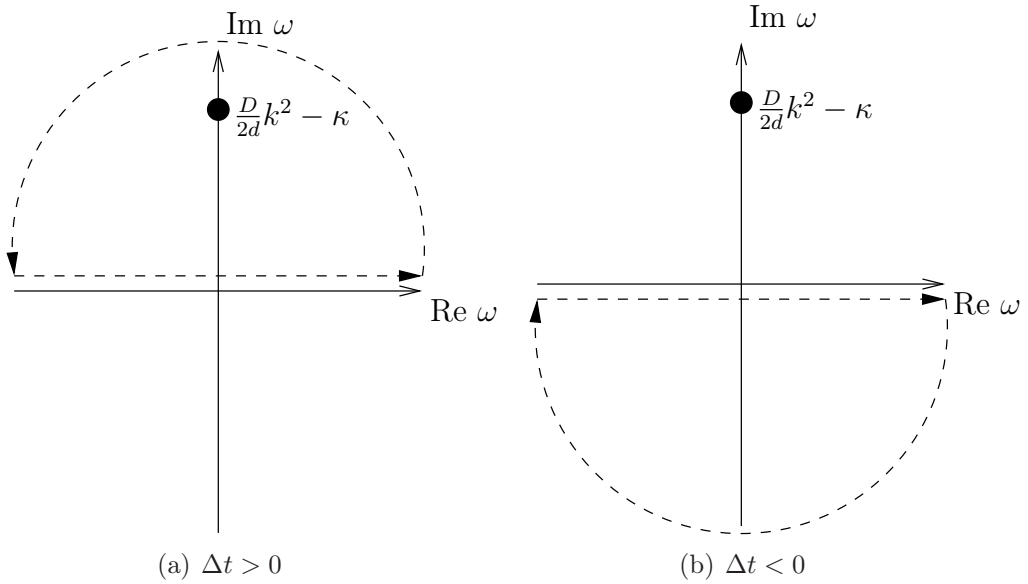
Figure 3.1.: Causality of the propagator (3.37): Depending on the value of the time argument the integration path has to be chosen in the upper or lower half of the complex plane. Therefore only certain momenta k contribute to the propagator. (The black point indicates the position of the pole)

can contribute to the integrals. At criticality, when $\kappa = 0$, the propagator is nonzero for the first case $\Delta t > 0$. Furthermore it does not vanish for large propagation lengths x as all momenta k are included. For nonzero κ the propagation length will be limited as low momenta are suppressed. In the second case $\Delta t < 0$ the propagator does not vanish in all cases. Indeed for non zero κ low momenta can contribute. This is not in conflict with causality as it just states, that if a particle annihilates in an over critical system a new particle will be created later at some point in the lattice. And this is true, as we know from simulations that the average particle density becomes a constant after a sufficient amount of time in such systems.

3.5.2. Interacting part

After deriving an exact result for the free field theory, we shall now turn towards the interacting terms. To this end we define a new functional by omitting the

3. Field-theoretical approach

integrals and the external currents in the nominator of (3.24)

$$\hat{Z}\left[\phi, \tilde{\phi}\right] = \frac{e^{-S}}{\int D\phi D\tilde{\phi} e^{-S}} \tag{3.44}$$

where S is the action

$$S = \int dx^d \, dt \, \mathcal{L} \tag{3.45}$$

of the system. Taking the variation of this functional with respect to ϕ and $\tilde{\phi}$ gives the coupled equations

$$\frac{\delta}{\delta\phi}\hat{Z}\left[\phi, \tilde{\phi}\right] = \left(\frac{\partial}{\partial t} + D\nabla^2 + \kappa\right)\tilde{\phi}\hat{Z}\left[\phi, \tilde{\phi}\right] - \left(\frac{\delta}{\delta\phi}\mathcal{L}_{int}\right)\hat{Z}\left[\phi, \tilde{\phi}\right] \tag{3.46}$$

$$\frac{\delta}{\delta\tilde{\phi}}\hat{Z}\left[\phi, \tilde{\phi}\right] = \left(-\frac{\partial}{\partial t} + D\nabla^2 + \kappa\right)\phi\hat{Z}\left[\phi, \tilde{\phi}\right] - \left(\frac{\delta}{\delta\tilde{\phi}}\mathcal{L}_{int}\right)\hat{Z}\left[\phi, \tilde{\phi}\right] \tag{3.47}$$

Multiplying them with $\exp\left(\int_{xt}\phi J + \tilde{\phi}\tilde{J}\right)$ and integrating over ϕ and $\tilde{\phi}$ leads to

$$JZ\left[J, \tilde{J}\right] =$$
$$\left(\frac{\partial}{\partial t} + D\nabla^2 + \kappa\right)\frac{\delta}{\delta\tilde{J}}Z\left[J, \tilde{J}\right] - \left(\frac{\delta}{\delta\phi}\mathcal{L}_{int}\right)\left[\frac{\delta}{\delta J}, \frac{\delta}{\delta\tilde{J}}\right]Z\left[J, \tilde{J}\right] \tag{3.48}$$

$$\tilde{J}Z\left[J, \tilde{J}\right] =$$
$$\left(-\frac{\partial}{\partial t} + D\nabla^2 + \kappa\right)\frac{\delta}{\delta J}Z\left[J, \tilde{J}\right] - \left(\frac{\delta}{\delta\tilde{\phi}}\mathcal{L}_{int}\right)\left[\frac{\delta}{\delta J}, \frac{\delta}{\delta\tilde{J}}\right]Z\left[J, \tilde{J}\right] \tag{3.49}$$

were the fields ϕ and $\tilde{\phi}$ have been replaced by $\frac{\delta}{\delta J}$ and $\frac{\delta}{\delta\tilde{J}}$. The solution of this equation system is

$$Z\left[J, \tilde{J}\right] = \frac{\exp\left(-\int_{xt}\mathcal{L}_{int}\left[\frac{\delta}{\delta J}, \frac{\delta}{\delta\tilde{J}}\right]\right)Z_0\left[J, \tilde{J}\right]}{\exp\left(-\int_{xt}\mathcal{L}_{int}\left[\frac{\delta}{\delta J}, \frac{\delta}{\delta\tilde{J}}\right]\right)Z_0\left[J, \tilde{J}\right]\Big|_{J,\tilde{J}=0}} \tag{3.50}$$

which is an exponential series in the coupling constant g.

We will not give a proof for this result at this point, as it would go far beyond the scope of this thesis. The interested reader may find in [12] how to derive and proof such a solution.

The denominator in (3.50) is chosen in way that the normalisation condition

$$Z\left[J, \tilde{J}\right]\Big|_{J,\tilde{J}=0} = 1 \tag{3.51}$$

holds true. In the next sections we will show, that for markovian processes this factor is always equal to one. This behaviour is caused by the non-reversibility of stochastic processes. We can therefore omit the denominator in the final generating functional. We end up with

$$Z\left[J, \tilde{J}\right] = \exp\left(-\int_{xt} \mathcal{L}_{int}\left[\frac{\delta}{\delta J}, \frac{\delta}{\delta \tilde{J}}\right]\right) Z_0\left[J, \tilde{J}\right]. \tag{3.52}$$

This generating functional can now be used to calculate observables of the diffusive contact process by functional variation. For this, the exponential in (3.52) has to be evaluated order by order. As the complexity of the involved equations increases with each order, it is usually not possible to find an expression for the whole exponential. Therefore it is common to calculate observables up to a certain order in coupling g. To ensure that this series expansion is sensible, the coupling g needs to be small enough.

3.6. Feynman rules for diffusive contact process

Because of the large mathematical expressions, which usually occur when calculating observables Feynman introduced a pictorial representation for propagators and interaction vertices. In this notation the propagator is usually represented by a line

$$\int_{xt} \int_{yt'} \tilde{J}(x,t)\,\bar{\Delta}_F(y-x, t'-t)\,J(y,t') = \tilde{J}(x,t) \underset{\rule{0pt}{0pt}}{\times\!\!-\!\!\!\longrightarrow\!\!\!-\!\!\times} J(y,t') \tag{3.53}$$

where the cross at each end of the line depicts the external current. In contrast to quantum field theory, the arrow indicates the direction of time.[3] Applying this rule to the nominator of (3.50) and expanding the exponential we obtain up to order g^2

$$Z^{(2)}\left[J, \tilde{J}\right] = \left(1 + z_1 + z_2 + \mathcal{O}\left(g^3\right)\right) \times \exp\left(\times\!\!-\!\!\!\longrightarrow\!\!\!-\!\!\times\right) \tag{3.54}$$

---

[3]In QFT the arrow usually represents the flow of charges.

for the functional. The superscripts remind us of the order of the functional. The first order and second order contributions z_1 and z_2 are given by

$$z_1 = -\frac{1}{1!} \int d^d x dt \, \mathcal{L}_{int} \left[\frac{\delta}{\delta J}, \frac{\delta}{\delta \tilde{J}} \right], \quad z_2 = \frac{1}{2!} \left(\int d^d x dt \, \mathcal{L}_{int} \left[\frac{\delta}{\delta J}, \frac{\delta}{\delta \tilde{J}} \right] \right)^2. \tag{3.55}$$

Computing the functional variations we find

$$z_1 = -\frac{g}{1!} \left(\text{} - \text{} \right) \tag{3.56}$$

$$z_2 = +\frac{g^2}{2!} \left(-4 \, \text{} - 8 \, \text{} - 2 \, \text{} + 4 \, \text{} \right.$$

$$\left. +4 \, \text{} + \text{} + \text{} - 2 \, \text{} \right) \tag{3.57}$$

for these two terms of the series expansion. We have omitted graphs like

$$\tag{3.58}$$

because they are zero due to causality.

At his point its sensible to show that the generating functional (3.54) is proper normalised or, in more general context, to explain why the denominator in (3.52) will always be one. If we set the external currents to zero, all graphs containing currents (depicted by the crosses) likewise become zero and therefor z_1 and z_2 will vanish. As the exponential becomes one, we find

$$Z^{(2)} \left[J, \tilde{J} \right] \bigg|_{J, \tilde{J} = 0} = 1 \tag{3.59}$$

for the generating functional. This proof can easily be extend to higher orders as follows. The only graphs which would not vanish upon setting J and $\tilde{J}$ zero are the closed loops. But these loops are zero due to causality. Therefore (3.52) will always be proper normalised. This result yields for all markovian

stochastic dynamics.

Using the expansion (3.54) it is now easy to calculate an arbitrary observable up to order g^2. For instance the two point correlation function which we already calculated for the free theory (3.41) reads now

$$
\begin{aligned}
C\left(y-x, t'-t\right) &= \frac{\delta}{\delta J\left(y, t'\right)} \frac{\delta}{\delta \tilde{J}\left(x, t\right)} Z^{(2)}\left[J, \tilde{J}\right]\bigg|_{J, \tilde{J}=0} \\
&= \bullet\!\!\longrightarrow\!\!\bullet \; - 2g^2 \; \bullet\!\!-\!\!\bigcirc\!\!-\!\!\bullet \\
&= \bar{\Delta}_F\left(y-x, t'-t\right) - 2g^2 \int_{r\tau} \int_{s\tau'} \times \qquad (3.60)\\
&\quad \bar{\Delta}_F\left(r-x, \tau-t\right) \bar{\Delta}_F^2\left(s-r, \tau'-\tau\right) \bar{\Delta}_F\left(y-s, t'-\tau'\right)
\end{aligned}
$$

with the loop being the second order contribution.

The previous introduced Feynman rules are valid in spatial space. A further simplification can be achieved by switching to Fourier space representation as the Lagrangian stays invariant under translation. For instance we have

$$
C\left(y-x, t'-t\right) = \int \frac{d^d k\, d\omega\, e^{-\imath(kx+\omega t)}}{(2\pi)^{(d+1)/2}} \int \frac{d^d k'\, d\omega'\, e^{-\imath(k'y+\omega' t')}}{(2\pi)^{(d+1)/2}} \left\langle \phi\left(k, \omega\right) \tilde{\phi}\left(k', \omega'\right) \right\rangle.
\tag{3.61}
$$

Because of translational invariance in space time we have

$$
k' = -k, \quad \omega' = -\omega
\tag{3.62}
$$

which expresses momentum conservation. We then have

$$
C\left(y'-x, t'-t\right) = \int \frac{d^d k\, d\omega}{(2\pi)^{d+1}} \exp^{\imath k(y-x)+\imath\omega(t'-t)} C\left(k, \omega\right)
\tag{3.63}
$$

where $C\left(k, \omega\right)$ is the two point correlation function in momentum space representation. As this translational invariance does not only hold for the whole correlation function but is also true at each interaction vertex, the sum of all momenta at a vertex is zero.

3. Field-theoretical approach

Transforming expression (3.60) into momentum space we find

$$C\left(k, \omega\right) = \Delta_F\left(k, \omega\right) \tag{3.64}$$
$$+ 2g^2 \Delta_F^2\left(k, \omega\right) \int \frac{d^d k' d\omega'}{(2\pi)^{d+1}} \Delta_F\left(\frac{k}{2} + k', \frac{\omega}{2} + \omega'\right) \Delta_F\left(\frac{k}{2} - k', \frac{\omega}{2} - \omega'\right) + \mathcal{O}\left(g^4\right)$$

for the two-point correlation function. This clearly shows the advantages of expressing observables in momentum space: much shorter and cleaner formula's. Therefore it is common to use wave vector and frequency instead of space and time coordinates.

Taking the previous computations into account, observables of the diffusive contact process can be expressed in terms of the following momentum space Feynman rules:

1. The diffusion and annihilation of particles, which is called propagation in the language of a field theory, is represented by an arrow which always points from $\tilde{\phi}$ to ϕ to remind the causal order:

$$\Delta_F\left(k, \omega\right) = \frac{1}{\frac{D}{2d}k^2 - \kappa - \imath\omega} = \quad \text{---} \blacktriangleright \text{---} \quad . \tag{3.65}$$
$$k, \omega$$

2. Interactions between particles are represented by vertices which correspond to a factor $\pm g$ in equations:

$$\text{---} \blacktriangleright \!\!\prec = g, \qquad \succ\!\!\blacktriangleright = -g \tag{3.66}$$

where the former vertex describes the creation of particles and the latter the boundary condition $\rho \leq 1$.

3. Additionally the topology of a graph leads to additional combinatorial factors which have to be taken into account:

   a) The faculty of the number of initial particles. (number of external $\tilde{\phi}$-fields)

   b) Faculty of number of final particles. (number of external ϕ fields)

   c) Each vertex with at least one internal line gets a factor 2.

d) A vertex which is connected with two lines to another vertex or to two incoming/two outgoing particles gets a factor of $1/2$ to account for twice counting.

4. Over indeterminate momenta, which usually occur in loops, has to be integrated with measure $\int d^d k d\omega \, (2\pi)^{-d-1}$.

3.7. One-Loop order of diffusive contact process

In the previous section we have derived the tools and equations needed for a field theoretic description of the diffusive contact process. The next step is to calculate the next order corrections, also called one loop contributions, to the propagator and interacting vertices.

As the non diffusive contact process is described by the same action, the following calculation is in its most parts similar to previous works. For instance, similar calculations can be found in [13, 4].

3.7.1. Propagator

The propagator (the two point correlation function) to one loop order reads in terms of Feynman rules

$$C\left(k,\omega\right) = \text{} \tag{3.67}$$

which, at first sight, does not look like one loop because of the series of concatenations of loops. However the term 'one loop' has to be understood in the context of vertex functions. Whereby the propagator is the inverse of the two point vertex function. Rewriting the geometrical series in (3.67) gives

$$C\left(k,\omega\right) = \left(\Gamma^{(1,1)}\left(k,\omega\right)\right)^{-1} \tag{3.68}$$

25

3. Field-theoretical approach

where we have introduced the two point vertex function

$$\Gamma^{(1,1)}(k,\omega) = \Delta_F^{-1}(k,\omega) - \quad \text{(diagram)} \tag{3.69}$$

which is clearly of one loop order. The superscript $(1,1)$ reminds to the number of initial and final particles.

Such vertex functions always contain only irreducible graphs. These are graphs which can not be split into two sub graphs by cutting a single line (like it is possible between the loops in (3.67)).

Replacing the pictographs by the associated formula elements the vertex function reads

$$\Gamma^{(1,1)}(k,\omega) = \Delta_F^{-1}(k,\omega) + 2g^2 \int \frac{d^d q \, d\nu}{(2\pi)^{d+1}} \Delta_F\left(\frac{k}{2}+q, \frac{\omega}{2}+\nu\right) \Delta_F\left(\frac{k}{2}-q, \frac{\omega}{2}-\nu\right) \tag{3.70}$$

where the second term corresponds to the one loop correction which we will compute in this section. In the following we denote the loop contribution

$$\text{(diagram)} = -2g^2 \int \frac{d^d q \, d\nu}{(2\pi)^{d+1}} \frac{1}{\frac{D}{2d}\left(\frac{k}{2}+q\right)^2 - \kappa + \imath\left(\frac{\omega}{2}+\nu\right)} \frac{1}{\frac{D}{2d}\left(\frac{k}{2}-q\right)^2 - \kappa + \imath\left(\frac{\omega}{2}-\nu\right)} \tag{3.71}$$

as $\Gamma_2^{(1,1)}(k,\omega)$. Carrying out the the frequency integral using the residue theorem gives the expression

$$\Gamma_2^{(1,1)}(k,\omega) = -4g^2 \int \frac{d^d q}{(2\pi)^d} \frac{1}{\frac{D}{2d}\left(4q^2 + k^2\right) - 4\kappa + 2\imath\omega}. \tag{3.72}$$

Counting the powers of q in the nominator and denominator shows, that the integral will diverge for $d \geq 2$. This result is very surprising, as we have pointed out before, that field theory should be the appropriate tool close to the critical dimension d_c. Therefore one expects[4] the divergence to enter the equations at this dimension, which is four in case of the directed percolation. Fortunately it turns out, that the loop contribution leads to a shift of the percolation threshold κ_c which in turn shifts the dimension, where the divergence appears in (3.72).

To account for this issue, we consider a general property of continuous phase transitions in association with a field theoretic requirement. At the phase

---

[4]Explanation follows later

26

transition correlation lengths diverge for continuous phase transitions. This corresponds to diverging zero momenta and zero frequency component of the two-point correlation function. Hence the condition

$$\Gamma^{(1,1)}(0,0) \overset{!}{=} 0 \tag{3.73}$$

must be fulfilled . We then find from (3.70)

$$\kappa_c = g^2 \int \frac{d^d q}{(2\pi)^d} \frac{1}{\frac{D}{2d}q^2 - \kappa_c} + \mathcal{O}\left(g^4\right) \tag{3.74}$$

which can be solved by iteration. To second order in g we find

$$\kappa_c = \frac{2dg^2}{D} \int \frac{d^d q}{(2\pi)^d} q^{-2} \tag{3.75}$$

corresponding to a non zero squared particle mass κ_c. But a field theory of a critical system is characterised by a zero particle mass. It is therefore necessary to replace κ by a squared mass

$$m = \kappa - \kappa_c + \mathcal{O}\left(g^4\right) \tag{3.76}$$

which is zero at the critical point. Inserting this result into (3.72) yields

$$\Gamma^{(1,1)}(k,\omega) = \frac{D}{2d}k^2 - m + \imath\omega - g^2 \int \frac{d^d q}{(2\pi)^d} \frac{\Delta^2}{\frac{D}{2d}q^2 \left(4\frac{D}{2d}q^2 + \Delta^2\right)} + \mathcal{O}\left(g^3\right) \tag{3.77}$$

where we used the abbreviation

$$\Delta^2 = \frac{D}{2d}k^2 - 4m + 2\imath\omega. \tag{3.78}$$

This expression now diverges for $d = 4$ as expected.

Again this divergence seems to break the field theory as observables would be infinity in four spatial dimensions. Indeed it will turn out later, that this divergence can be absorbed by choosing a different set of fields and parameters and is closely related to the scaling behaviour of the diffusive contact process.

For this purpose it is necessary to extract the diverging part of the integral. To this end we use a procedure called dimensional regularisation, which is

based on the observation, that the integral does not diverge for $d < 4$. Using the Γ-function which can be defined as a d-dimensional integral

$$\int d^d q \frac{q^r}{(q^2+1)^s} = \pi^{d/2} \frac{\Gamma\left(\frac{d+r}{2}\right)\Gamma\left(s-\frac{d+r}{2}\right)}{\Gamma\left(d/2\right)\Gamma\left(s\right)} \quad \text{for} \quad r \leq 2s - d \qquad (3.79)$$

(3.72) can be expressed as a function of the dimension d. Here d does not need to be an integral number anymore. We then have

$$\Gamma^{(1,1)}(k,\omega) = \frac{D}{8-2\epsilon}k^2 - m + \imath\omega + \frac{g^2\mu^{-\epsilon}\Delta^2}{64\pi^2\left(\frac{D}{8-2\epsilon}\right)^2}\left(\frac{\Delta^2}{16\pi\mu^2\frac{D}{8-2\epsilon}}\right)^{-\frac{\epsilon}{2}}\Gamma\left(\frac{\epsilon}{2}-1\right)$$
$$(3.80)$$

where $\epsilon = 4 - d$. Furthermore we have introduced a momentum scale μ to keep the term within the brackets dimensionless. This is necessary to expand this term in powers of ϵ:

$$\Gamma_2^{(1,1)}(k,\omega) = -\frac{g^2\mu^{-\epsilon}\Delta^2}{64\pi^2\left(\frac{D}{8-2\epsilon}\right)^2}\left(-\frac{2}{\epsilon}+\left(\gamma-1+\ln\frac{\Delta^2}{16\pi\mu^2\frac{D}{8-2\epsilon}}\right)+\mathcal{O}\left(\epsilon\right)\right)$$
$$(3.81)$$

where the divergent part shows up as a well defined $1/\epsilon$ contribution.

3.7.2. Vertices

Before we can proceed with the renormalisation procedure, it is necessary to calculate the one loop correction of the interaction vertices as well. Fortunately it is sufficient to concern only one of the two vertices as they are symmetric under time reversal and field swapping as show in section 3.3.

To one loop order we have

$$\Gamma^{(1,2)}(k,\omega,k',\omega') = \quad\text{} \qquad (3.82)$$

where the index indicate the momentum flow.

In the previous section it turned out that loops contain divergent contributions. As the scaling behaviour is fully governed by these divergences, the calculation can be significantly simplified by neglecting the finite contributions.

we therefore set external momenta and frequencies to zero and obtain

$$\Gamma^{(1,2)}\left(0,0,0,0\right) = 2g - 16g^3 \int \frac{d^d q d\nu}{(2\pi)^{d+1}} \Delta_F^2\left(q,\nu\right) \Delta_F\left(-q,-\nu\right). \qquad (3.83)$$

Writing out the propagators and replacing κ by m gives

$$\Gamma^{(1,2)}\left(0,0,0,0\right) = 2g - 16g^3 \int \frac{d^d q d\nu}{(2\pi)^{d+1}} \frac{1}{\left(\frac{D}{2d}q^2 - m + \imath\nu\right)^2 \left(\frac{D}{2d}q^2 - m - \imath\nu\right)}. \qquad (3.84)$$

Here the shift κ_c computed in the previous section can be omitted as it would lead to corrections of order $\mathcal{O}\left(g^4\right)$ which are of higher precision than the one loop contributions.

Using the residue theorem to compute the frequency integral and inserting the Γ-function (3.79) we find

$$\Gamma^{(1,2)}\left(0,0,0,0\right) = 2g + g^3 \frac{\left(2-\epsilon\right)\mu^{-\epsilon}}{2\pi^2 m^2} \left(-\frac{m}{2\pi\mu^2 \frac{D}{2di}}\right)^{-\epsilon/2} \Gamma\left(\frac{\epsilon}{2}\right) \qquad (3.85)$$

where again $\epsilon = 4 - d$ is the deviation from the critical dimension and μ stands for a momentum scale. Expanding this expression in orders of ϵ

$$\Gamma_2^{(1,2)}\left(0,0,0,0\right) = 2g - \frac{g^3\mu^{-\epsilon}}{2\pi^2\left(\frac{D}{8-2\epsilon}\right)^2 \epsilon} + \frac{g^3\mu^{-\epsilon}}{4\pi^2\left(\frac{D}{8-2\epsilon}\right)^2} \left(\gamma_e - \ln\frac{-m}{4\pi\mu^2\left(\frac{D}{8-2\epsilon}\right)}\right) + \mathcal{O}\left(\epsilon\right) \qquad (3.86)$$

yields the desired divergent part. The negative sign in the logarithm stems from the simplification made above and would disappear if external momenta are applied.

3.8. Renormalisation

In the previous sections it turned out that when calculating the second order corrections to the propagator and vertex functions, divergences show up. They are caused by the fact that the field theoretic description neglects the lattice structure of the underlying system. Therefore the loop momenta are not bounded by the lattice spacing as they should. Fortunately these divergences can be absorbed by an appropriate redefinition of fields and parameters. This

3. Field-theoretical approach

procedure is called renormalisation. Furthermore it turns out that the new fields and parameters obtain corrections to their scaling behaviour which lead to modifications of the mean field scaling exponents.

Starting from the original Lagrangian (3.21) we rename all fields and parameters as bare values denoted by subscript "0"

$$\mathcal{L}_0 = \frac{1}{2}\left(\phi_0\frac{\partial}{\partial t}\phi_0 - \phi_0\frac{\partial}{\partial t}\tilde{\phi}_0\right) + D_0(\nabla\tilde{\phi}_0)(\nabla\phi_0) - m_0\phi_0\tilde{\phi}_0 + g_0\left(\tilde{\phi}_0\phi_0^2 - \tilde{\phi}_0^2\phi_0\right). \tag{3.87}$$

We now relate these bare values to physical parameters and fields by introducing Z-factors. Setting

$$\phi_0 = \sqrt{Z_\phi}\phi, \ \tilde{\phi}_0 = \sqrt{Z_{\tilde{\phi}}}\tilde{\phi}, \ D_0 = Z_D D, \ \kappa_0 = Z_m m, \ g_0 = Z_g g. \tag{3.88}$$

Because of the time reversal symmetry described in section 3.3 we have

$$Z_{\tilde{\phi}} = Z\phi \tag{3.89}$$

for the diffusive contact process. Setting $Z_i = 1 + \delta Z_i$ and neglecting quadratic and higher powers of δZ_i which would be of higher order in the coupling g yields the Lagrangian

$$\mathcal{L} = \mathcal{L}\left(\phi, \tilde{\phi}, D, m, g\right) \tag{3.90}$$

$$+\delta Z_\phi\frac{1}{2}\left(\tilde{\phi}\frac{\partial}{\partial t}\phi - \phi\frac{\partial}{\partial t}\tilde{\phi}\right) \tag{3.91}$$

$$+ \left(\delta Z_D + \delta Z_\phi\right)\frac{D}{2d}(\nabla\tilde{\phi})(\nabla\phi) \tag{3.92}$$

$$- \left(\delta Z_\phi + \delta Z_m\right)m\phi\tilde{\phi} \tag{3.93}$$

$$+ \left(\frac{3}{2}\delta Z_\phi + \delta Z_g\right)g\left(\tilde{\phi}\phi^2 - \tilde{\phi}^2\phi\right). \tag{3.94}$$

This expression contains besides the known parts additional so called counter terms. They lead to new elements in the field theory and are usually treated as interaction vertices as they depend on the coupling g. In terms of Feynman rules these read:

Propagator counter vertex

$$\text{--►✳-►--} \quad = -\left(\delta Z_D + \delta Z_\phi\right)\frac{D}{2d}k^2 + \left(\delta Z_\phi + \delta Z_m\right)m - \imath\delta Z_\phi\omega$$

(3.95)

Interaction counter vertices

$$\text{--►✳◄} \quad = +2\left(\frac{3}{2}\delta Z_\phi + \delta Z_g\right)g \qquad (3.96)$$

$$\text{►✳-►--} \quad = -2\left(\frac{3}{2}\delta Z_\phi + \delta Z_g\right)g \qquad (3.97)$$

These new terms lead to further contributions to the propagator and interaction vertices which have to be taken in account. We then have

$$\Gamma^{(1,1)}\left(k,\omega\right) = \text{●--►--●} - \text{►●◉●►} - \text{--►✳-►-} \qquad (3.98)$$

for the inverse propagator and

$$\Gamma^{(1,2)}\left(k,\omega,k',\omega'\right) = \text{-►◄} + \text{►●◄} + \text{--►✳◄} \qquad (3.99)$$

for the three-point vertex function. Writing out these pictographs we find

$$\Gamma^{(1,1)}\left(k,\omega\right) = \left(\frac{D}{2d}k^2 - m + \imath\omega\right) - \frac{u}{\epsilon}\left(\frac{D}{2d}k^2 - 4m + 2\imath\omega\right)$$
$$+ \left(\delta Z_D + \delta Z_\phi\right)\frac{D}{2d}k^2 - \left(\delta Z_\phi + \delta Z_m\right)m + \imath\delta Z_\phi\omega + \text{finite} + \mathcal{O}\left(\epsilon\right) \tag{3.100}$$

and

$$\Gamma^{(1,2)}\left(0,0,0,0\right) = 2g - 16g\frac{u}{\epsilon} + 2\left(\frac{3}{2}\delta Z_\phi + \delta Z_g\right)g + \text{finite} + \mathcal{O}\left(\epsilon\right). \quad (3.101)$$

where we summarised the non divergent one loop contributions as "finite" and introduced an effective coupling

$$u = \frac{g^2 \mu^{-\epsilon}}{32\pi^2 \left(\frac{D}{2d}\right)^2}, \quad u = \frac{Z_D^2}{Z_g^2} \mu^{-\epsilon} u_0. \tag{3.102}$$

If we now choose the renormalisation factors as

$$\delta Z_\phi = \frac{2u}{\epsilon}, \quad \delta Z_D = -\frac{u}{\epsilon}, \quad \delta Z_m = \frac{2u}{\epsilon}, \quad \delta Z_g = \frac{5u}{\epsilon} \tag{3.103}$$

the divergences are cancelled by the counter terms. The renormalised propagator and interaction vertices are now finite.

Due to these counter terms, observables can computed up to one loop order now. For higher loop order calculations the renormalisation procedure has to be repeated and gives further higher order counter terms.

3.8.1. Scaling properties

The previous calculations made it necessary to introduce a momentum scale μ. However, when computing observables using the bare Lagrangian there would not be such a momentum scale. Therefore equation

$$0 \overset{!}{=} \mu \frac{d}{d\mu} \Gamma_0^{\left(N,\tilde{N}\right)} \left(D_0, g_0, m_0, k, \omega, k', \omega' \dots\right) \tag{3.104}$$

must be fulfilled. Using the renormalisation prescriptions (3.88) we can relate unrenormalised and renormalised vertex functions to each other. We find

$$\Gamma_0^{\left(N,\tilde{N}\right)} = Z_\phi^{\left(N+\tilde{N}\right)/2} \Gamma^{\left(N,\tilde{N}\right)} \tag{3.105}$$

which inserted into (3.104) gives the differential equation

$$0 \overset{!}{=} \mu \frac{d}{d\mu} Z_\phi^{\left(N+\tilde{N}\right)/2} \Gamma^{\left(N,\tilde{N}\right)} \left(\mu, D, u, m, k, \omega, k', \omega' \dots\right) \tag{3.106}$$

for the renormalised vertex functions. Applying chain rule yields

$$0 = \left(\mu \frac{\partial}{\partial \mu} + \frac{N + \tilde{N}}{2} \gamma_\phi + \gamma_D D \frac{\partial}{\partial D} + \gamma_m m \frac{\partial}{\partial m} + \beta \frac{\partial}{\partial u}\right) \Gamma^{\left(N,\tilde{N}\right)} \left(\cdots\right) \tag{3.107}$$

where we have introduced the flow functions

$$\beta = \mu \frac{du}{d\mu} = \mu \frac{du_0 \mu^{-\epsilon} Z_D^2 Z_g^{-2}}{d\mu} = -\epsilon u + 12u^2 + \mathcal{O}\left(u^3\right) \qquad (3.108)$$

$$\gamma_\phi = \frac{\mu}{Z_\phi} \frac{dZ_\phi}{d\mu} = \frac{2}{\epsilon} \cdot \beta = -2u + \mathcal{O}\left(u^2\right) \qquad (3.109)$$

$$\gamma_D = \frac{\mu}{D} \frac{dD}{d\mu} = -u + \mathcal{O}\left(u^2\right) \qquad (3.110)$$

$$\gamma_m = \frac{\mu}{m} \frac{dm}{d\mu} = \frac{\mu}{m} \frac{dm_0 Z_m^{-1}}{d\mu} = +2u + \mathcal{O}\left(u^2\right) \qquad (3.111)$$

for parameters and fields. This differential equation system can be solved using the method of characteristics. For this we extract the dimension of the vertex-function as

$$\Gamma^{(N,\tilde{N})}\left(\mu, D, u, m, k, \omega, k', \omega' \ldots\right) = \mu^{\left[\Gamma^{(N,\tilde{N})}\right]} \hat{\Gamma}^{(N,\tilde{N})}\left(1, D, u, \frac{m}{D\mu^2}, \frac{k}{\mu}, \frac{\omega}{D\mu^2}, \ldots\right)$$
$$(3.112)$$

where we defined $\hat{\Gamma}^{(N,\tilde{N})}$ as a dimensionless function. Here the form of the scale free arguments has been obtained by splitting the inverse propagator as

$$\Delta_F^{-1}(k, \omega) = \frac{D}{2d}\mu^2 \cdot \left(\left(\frac{k}{\mu}\right)^2 - \frac{2d}{D\mu^2}m + \imath\frac{2d}{D\mu^2}\omega\right) \qquad (3.113)$$

where the second term is scale free.

Introducing a dilatation factor l where

$$\tilde{\mu}(l) = \mu l \qquad (3.114)$$

and regarding $\tilde{m}$, $\tilde{D}$ and $\tilde{u}$ as functions of l instead of μ we again employ the chain rule and obtain

$$0 = \left(-l\frac{d}{dl} + l\frac{d\tilde{D}}{dl}\frac{\partial}{\partial D} + l\frac{d\tilde{m}}{dl}\frac{\partial}{\partial m} + l\frac{d\tilde{u}}{dl}\frac{\partial}{\partial u}\right)\hat{\Gamma}^{(N,\tilde{N})}(\ldots). \qquad (3.115)$$

3. Field-theoretical approach

Comparing this result with (3.107) we find a set of differential equations

$$l\frac{d}{dl}\ln\hat{\Gamma}^{(N,\tilde{N})}(l) = \left(-\left[\Gamma^{(N,\tilde{N})}(\cdots)\right] - \frac{N+\tilde{N}}{2}\gamma_\phi(l)\right) \quad (3.116)$$

$$l\frac{d}{dl}\ln\tilde{D}(l) = \gamma_D(l) \quad \tilde{D}(1) = D \quad (3.117)$$

$$l\frac{d}{dl}\ln\tilde{m}(l) = \gamma_m(l) \quad \tilde{m}(1) = m \quad (3.118)$$

$$l\frac{d}{dl}\tilde{u}(l) = \beta(l) \quad (3.119)$$

where the l dependence of flow functions on the right hand side can be expressed in terms of the effective coupling $u(l)$ as shown in (3.108 - 3.111). Separating the variables and integrating leads to the formal solutions

$$\hat{\Gamma}^{(N,\tilde{N})}(l) = \hat{\Gamma}^{(N,\tilde{N})}(1)\, l^{-\left[\Gamma^{(N,\tilde{N})}(\cdots)\right]}\exp\left(-\frac{N+\tilde{N}}{2}\int_1^l dl\,\frac{\gamma_\phi(l)}{l}\right) \quad (3.120)$$

$$\tilde{D}(l) = \tilde{D}(1)\exp\left(\int_1^l dl\,\frac{\gamma_D(l)}{l}\right) \quad (3.121)$$

$$\tilde{m}(l) = \tilde{m}(1)\exp\left(\int_1^l dl\,\frac{\gamma_m(l)}{l}\right) \quad (3.122)$$

$$\tilde{u}(l) - \tilde{u}(1) = \int_1^l dl\,\frac{\beta(l)}{l} \quad (3.123)$$

for this equations.

Observing that scale invariance is only possible if the rescaling factors only depend on the change in the dilatation l and not on the value of l itself, the flow functions must be independent from l. Otherwise the integrals in (3.120 - 3.123), which are the rescaling factors, would depend on the value of l. Consequently the coupling $u(l)$ must be a constant which can be expressed as condition

$$0 \stackrel{!}{=} \beta(l) = \beta(u(l)) \quad (3.124)$$

on the β-function. This equation has two solutions, one trivial with zero coupling and the non trivial one

$$u^* = \frac{\epsilon}{12} + \mathcal{O}\left(\epsilon^2\right). \quad (3.125)$$

34

which leads to the constant anomalous dimensions

$$\gamma_\phi^* = -\frac{1}{6}\epsilon + \mathcal{O}\left(\epsilon^2\right) \tag{3.126}$$

$$\gamma_D^* = -\frac{1}{12}\epsilon + \mathcal{O}\left(\epsilon^2\right) \tag{3.127}$$

$$\gamma_m^* = +\frac{\epsilon}{6} + \mathcal{O}\left(\epsilon^2\right). \tag{3.128}$$

Inserting this results into the integrals (3.116-3.119) we find

$$\hat{\Gamma}^{(N,\tilde{N})}(l) = \hat{\Gamma}^{(N,\tilde{N})}(1) l^{-\left[\Gamma^{(N,\tilde{N})}(\dots)\right]-\frac{N+\tilde{N}}{2}\gamma_\phi^*} \tag{3.129}$$

$$\tilde{D}(l) = \tilde{D}(1) l^{\gamma_D^*} \tag{3.130}$$

$$\tilde{m}(l) = \tilde{m}(1) l^{\gamma_m^*} \tag{3.131}$$

$$\tilde{u}(l) = \tilde{u}^* \tag{3.132}$$

for the scaling behaviour of the parameters and vertex functions. Collecting all terms a general renormalised vertex function reads

$$\Gamma^{(N,\tilde{N})}(\mu, q, \omega, m, D, u) = \tag{3.133}$$
$$\mu^{\Gamma^{(N,\tilde{N})}} l^{\left[\Gamma^{(N,\tilde{N})}\right]+\frac{N+\tilde{N}}{2}\gamma_\phi^*} \hat{\Gamma}\left(1, \frac{q}{\mu}l^{-1}, \frac{\omega}{D\mu^2}l^{-2-\gamma_D^*}, \frac{m}{D\mu^2}l^{-2+\gamma_m^*-\gamma_D^*}, Dl^{\gamma_D^*}, u^*\right)$$

where the scaling behaviour shows up in terms of dilatation l. Inverse Fourier transformation and setting $l = t^{-\frac{1}{2+\gamma_D^*}}$ we find that a generic vertex function can always be written as

$$\Gamma^{(N,\tilde{N})}(x, t, m, D) \sim t^{-\frac{\left[\Gamma^{(N,\tilde{N})}\right]+\frac{N+\tilde{N}}{2}\gamma_\phi^*}{2+\gamma_D^*}} \hat{\Gamma}\left(xt^{-\frac{1}{2+\gamma_D^*}}, mt^{\frac{2-\gamma_m^*+\gamma_D^*}{2+\gamma_D^*}}, Dt^{-\frac{\gamma_D^*}{2+\gamma_D^*}}\right)$$
$$\tag{3.134}$$

where x and t represent a certain length and time variable of the function. From this equation we read off the scaling exponents

$$z = 2 - \epsilon/12 + \mathcal{O}\left(\epsilon^2\right), \quad \nu_\parallel = 1 + \epsilon/12 + \mathcal{O}\left(\epsilon^2\right), \quad \nu_\perp = 1/2 + \epsilon/16 + \mathcal{O}\left(\epsilon^2\right) \tag{3.135}$$

and the diffusive scaling exponent

$$\alpha = \epsilon/24 + \mathcal{O}\left(\epsilon^2\right). \tag{3.136}$$

3. Field-theoretical approach

Reminding that $\rho \sim \Gamma^{(1,0)}$ the last exponent is

$$\beta = 1 - \epsilon/6 + \mathcal{O}\left(\epsilon^2\right) \qquad (3.137)$$

These results are equal to the directed percolation exponents. Therefore introducing diffusion does not change the universality class, neither the scaling exponents are influenced by the diffusion constant. This result is not surprising as diffusion does not change the geometric properties of a system.

3.9. Crossover-Exponent

In the last section of this chapter, we will focus on the question how the diffusion rate D changes the critical creation rate λ_c. To this end we consider the field theoretic calculation at the beginning. Due to conceptional problems of the critical field theory, we had to replace the parameter κ by mass $m = \kappa - \kappa_c\left(D\right)$ where the shift is defined by equation

$$\kappa_c = g^2 \int \frac{d^d q}{(2\pi)^d} \frac{1}{\frac{D}{2d}q^2 - \kappa_c} \quad \text{with } \sqrt{2d\kappa_c/D} < |q| < \Omega. \qquad (3.138)$$

It was chosen in a way that m is zero at criticality. The lower boundary is given by the fact, that for q smaller than $\sqrt{2d\kappa_c/D}$ the propagator becomes zero. The upper boundary Ω is a cutoff scale in momentum space and should be sent to infinity under continued renormalisation. Inserting the d-dimensional surface element and expanding the right hand side of (3.138) in powers of q one obtains an integral over a geometric series

$$\kappa_c = \frac{4dg^2}{(4\pi)^{d/2} D\Gamma\left(d/2\right)} \int_{\sqrt{2d\kappa_c/D}}^{\Omega} dq\, q^{d-3} \sum_{i=0}^{\infty} \left(\frac{2dq^{-2}\kappa_c}{D}\right)^i. \qquad (3.139)$$

By dimensional analysis it is easy to see that for $d < 2$ only the lower boundary and for $d > 2$ only the upper boundary contributes to the integral. This behaviour can be explained by considering the probability of return of an ordinary random walk. Below two spatial dimensions this probability is non zero. Therefor particles stay close to each other. As the amount of successful creation operations depends on the number of surrounding particles, a change in the dif-

fusion constant leads to large changes in the percolation threshold. In contrast to that, higher spatial dimensions lead to zero return probability. Here the particles spread over the whole system and can not inhibit the creation process that strong.

Unfortunately it is not possible to find an analytical solution of (3.139). But for large diffusion constants we can approximate the sum by the leading term. Integrating the remaining part yields

$$\lambda_c (D) - 1 \sim \begin{cases} D^{-\frac{d}{4-d}} & \text{for } d < 2 \\ \frac{\log D}{D} & \text{for } d = 2 \\ D^{-1} & \text{for } d > 2 \end{cases} . \tag{3.140}$$

for the crossover behaviour.

This result clearly shows that the percolation threshold approaches the mean field prediction upon increasing diffusion rate. In terms of a crossover exponent

$$\lambda_c (D) - 1 \sim D^{-1/\phi(d)} \tag{3.141}$$

we find from (3.140) the values

$$\phi (d) = \begin{cases} 3 & \text{for } d = 1 \\ 1 + \text{log. corrections} & \text{for } d = 2 \\ 1 & \text{for } d \geq 3 \end{cases} . \tag{3.142}$$

These results clearly show, that an increase of the diffusion rate turns the critical creation rate down to the mean field prediction. This agrees with the phenomenological proposal, that diffusion enhances the mixing between the lattice sites. Hence local fluctuation are suppressed and the system becomes more mean field like. For $d \geq 2$ the exponents which describes the crossover becomes a constant which can be understand by reminding that the probability of return of a random walk becomes zero for $d \geq 2$.

Our results compare very well to the predictions already made in [8] where geometrical arguments are used to derive this result. However, an advantage of our solution is its simple and direct way. Furthermore it is easy to extend this calculation to other stochastic processes.

3. Field-theoretical approach

4. Monte Carlo simulation

4.1. Introduction

Beneath the analytical treatment of the diffusive contact process we used numerical simulations to obtain estimates for the various exponents and in order to support the results of our calculations. To this end, we used a Monte-Carlo algorithm to simulate the diffusive contact process and measured the particle density as a function of time for many different values of the parameters creation rate λ, diffusive mixing D, spatial dimension d and lattice size. Afterwards we determined the critical percolation threshold and the scaling exponents from these data. We used the methods described in [4] for this purpose:

1. To obtain estimates for the percolation threshold λ_c, exponents δ and $\nu_\parallel$ it is necessary to avoid finite size effects. These occur when spatial correlation lengths exceed the systems size. Therefore the time evolution of the particle density has been measured using as large as possible systems to suppress these influences.

   Unfortunately, as correlation lengths diverge close to the phase transition the achievable lattice size limits the precision of the estimates.

2. In contrast to that, finite size effects can be utilised to extract the third exponent $z = \nu_\parallel/\nu_\perp$. For this purpose simulations are done at the critical point $(\lambda = \lambda_c)$ for different system sizes.

To extract proper values for the desired exponents, we used simulation times up to 10^7 time steps. Together with the large lattice sizes of up to 2^{21} sites this leads to up to 10^{13} Monte-Carlo updates corresponding to several days computing time per single simulation run. In addition to that, we had to average the density curves over several ensembles of independent runs to obtain smooth curves and suppress statistic fluctuations.

Besides this Monte-Carlo approach we used *Mathematica*® to integrate equation (3.138) numerically which directly leads to critical curves. While this integration becomes unstable for small diffusion constants, it can be used to obtain reasonable results for large diffusion rates where the Monte-Carlo takes too much time.

4.2. Simulation application

In this section, we will give a more detailed description of the application we used for the simulation of the diffusive contact process. As already written in the previous section our kind of simulations consumes a large amount of CPU time. To address this issue, we used a client-server model where a server application was responsible for distributing the simulation parameters among the clients and retrieving and storing the results they returned.

To model the dynamics of the diffusive contact process, we used a Monte-Carlo algorithm which performs random sequential updates on a cubic d-dimensional space lattice with periodic boundaries. Figure 4.1 shows the flow chart of the central update function, which advances the system by a small step in time on each execution. On every micro-update, this algorithm selects a random lattice site and if this site is occupied by a particle, one of the following moves is performed:

- Remove the particle with probability $1/(1 + \lambda + D)$.

- Create a particle on a randomly chosen neighbouring site if this site is empty with probability $\lambda/(1 + \lambda + D)$.

- Move the particle with probability $D/(1 + \lambda + D)$ to a randomly selected neighbouring site if this site is empty.

After that, independent of whether an update succeeded or not, the time is increased by $dt = 1/(1 + \lambda + D)/N$ where N is the number of lattice sites.

To measure the evolution of density, we start with an initially fully occupied lattice and apply the update function several times. While that we count the particles on the lattice at exponentially distributed[1] time points and compute

---

[1]As we use logarithmic plots for the evaluation we saved a lot of disk space with this technique.
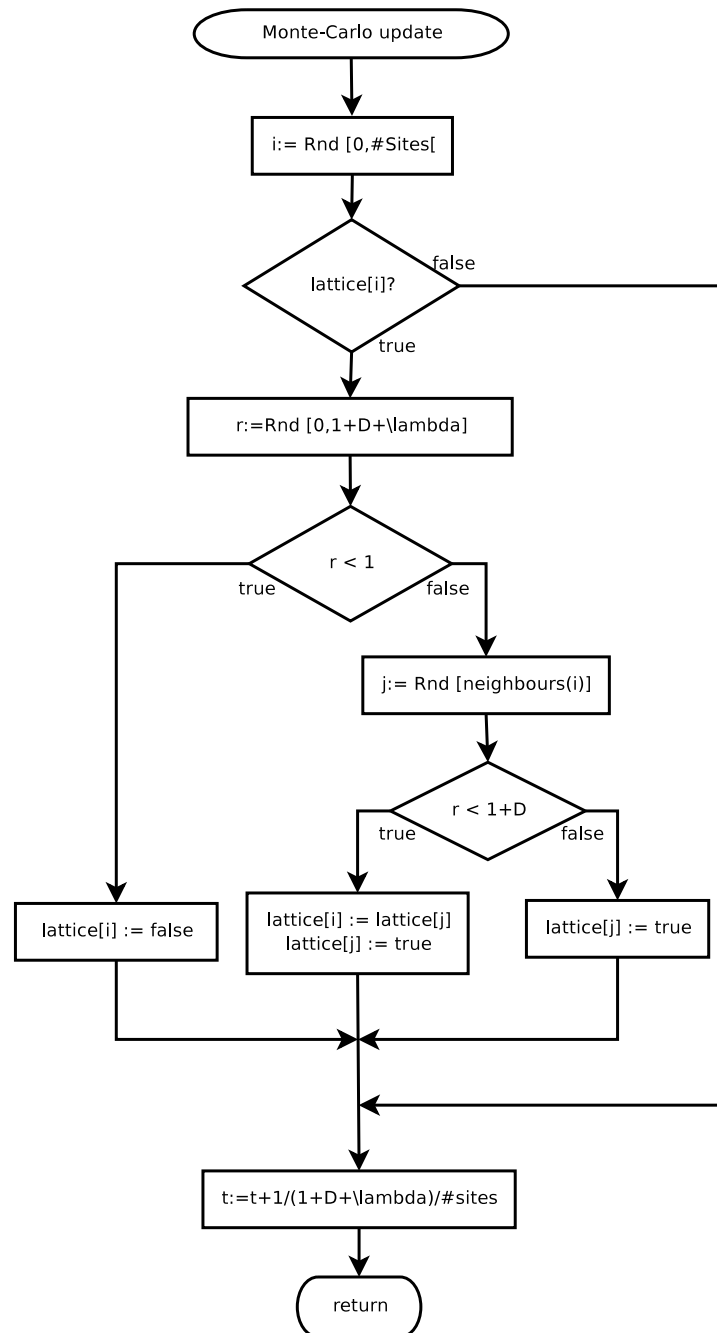
Figure 4.1.: Simplified flow chart of the update sequence used for our Monte Carlo simulations. Items: *lattice[]:* Boolean array representing the cubic lattice; *Rnd:* function creating a random number in a given interval using the algorithm presented in [16];

4. Monte Carlo simulation

Table 4.1.: Parameter ranges for which we have simulated the diffusive contact process in order to obtain estimates for the percolation threshold λ_c, the exponents δ and $\nu_\parallel$ and the crossover behaviour.

dimension	lattice sizes	creation rate	diffusion constant
1	65535^1	$[1, 3.3]$	$[0, 700]$
2	256^2, 512^2, 1024^2	$[1.003, 1.6875]$	$[0, 700]$
3	32^3, 64^3, 128^3	$[1.0001, 1.3203]$	$[0, 400]$
4	16^4, 32^4	$[1.0, 1.4]$	$[0, 100]$

Table 4.2.: Parameter ranges for finite size simulations which have been used to determine the third exponent z. These simulations are always done at criticality. $(\lambda = \lambda_c)$

dimension	lattice sizes	diffusion constant
1	16^1, 32^1, 64^1, 128^1, 256^1, 512^1, 1024^1, 2048^1	$[0, 700]$
2	4^2, 8^2, 16^2, 32^2, 64^2, 128^2	$[0, 700]$
3	2^3, 4^3, 8^3, 16^3, 32^3	$[0, 400]$
4	2^4, 4^4, 8^4, 16^4	$[0, 100]$

the density of particles from this number. The result of such a run is a density-time curve for a certain choice of parameters. Because of the limited system size and stochastic nature of this process, each simulation has to be repeated several times with the same parameters whereby the final density-time function is an average of each ensemble of runs.

Using this set up we have simulated the diffusive contact process for several hundred sets of parameters which cover the parameter ranges shown in table 4.1 and 4.2.

Before discussing the results in detail, we should note that most of the exponents we will present in the following, have already determined to much higher precision in previous works [7, 6, 14] for non diffusive systems. In certain cases our estimates don't compare very well to these results. However, as our idea was to study the influence of diffusion on the contact process it is not sensible to determine exponents and thresholds to high precision. Indeed the dependence on changes in the diffusion rate is quite of more interest.
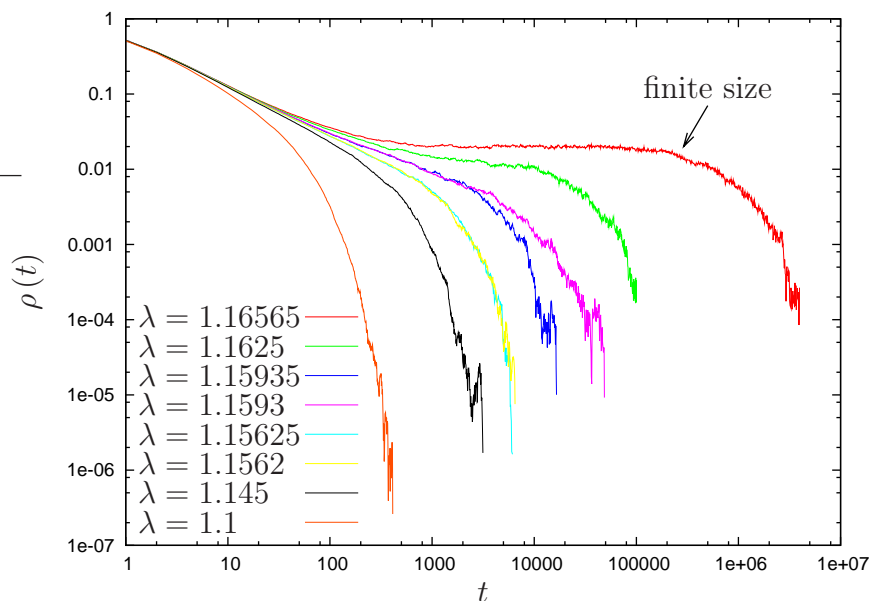
Figure 4.2.: Time development of the particle density of a $2 + 1$-dimensional system shown in a double-logarithmic plot. The particle density saturates in the super critical regime (green and red) and decays exponentially for sub-critical parameters (orange to turquoise). Also the super-critical regime clearly shows finite size effects. (Simulation parameters: Diffusion constant $D = 20$ fixed and lattice since as large as sensible.)

4.3. Percolation threshold

In order to extract the scaling and the crossover exponents from the numerical data obtained by simulations, we need to know the critical creation rate. To this end, density curves with equal diffusion rates are compared in a double-logarithmic graph as shown in figure 4.2. In such a plot, super critical curves are characterised by either the density approaching a constant value or at least by a slower then power law decay if finite size effects occur. (the red and green lines in fig. 4.2) In contrast to that, sub-critical curves show a stronger, usually exponential, decay than a power law (orange and black in fig. 4.2). Now, taking into account that the critical curve is always enclosed by super- and sub-critical curves, an upper and lower boundary for the percolation threshold can be estimated.

The accuracy of this method is limited by its sensibility to finite size effects which become important whenever correlation lengths grow beyond the system

4. Monte Carlo simulation
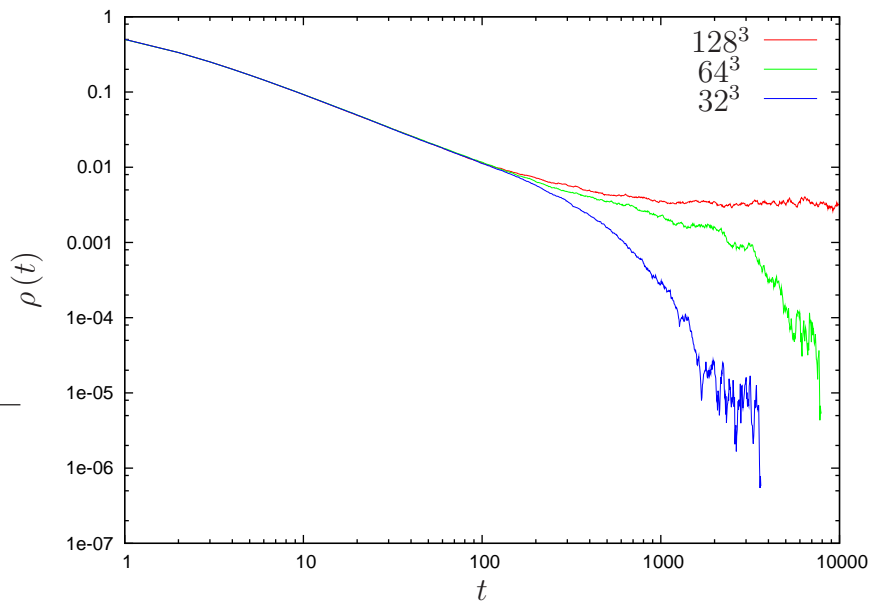
Figure 4.3.: The plot shows the evolution of the particle density for different lattice sites to evince finite size effects. Although the parameters are chosen to be in the super-critical regime, small systems show a sub-critical behaviour for density (blue line). (Fixed simulation parameters $d = 3$, $D = 200$ and $\lambda = 1.006$)

size. For instance figure 4.3 shows the simulation results for the same choice of parameters but different system sizes. Here the blue graph may be considered sub-critical, the green is something in between and the red one shows the correct overcritical behaviour. To detect these effects we simulated apparently sub-critical curves again on bigger systems whenever it was possible.

The phase diagrams we derived with this method are presented in figure 4.4. These plots clearly indicate the suggested behaviour, that the critical creation rate approaches the mean field prediction for large diffusion constants. Indeed for small diffusion rates, the percolation threshold stays above the mean field value. This happens also for spatial dimensions greater than four, which shows that a mean field description, even above the critical dimension, is not sufficient to determine the percolation threshold of the diffusive contact process.

It is possible to understand this behaviour by considering the particle creation mechanism. As new particles are created as neighbours of existing particles, a small part of subsequent creation operations will fail. Therefore the effective creation rate tends to be smaller than λ. But the mean field approach neglects
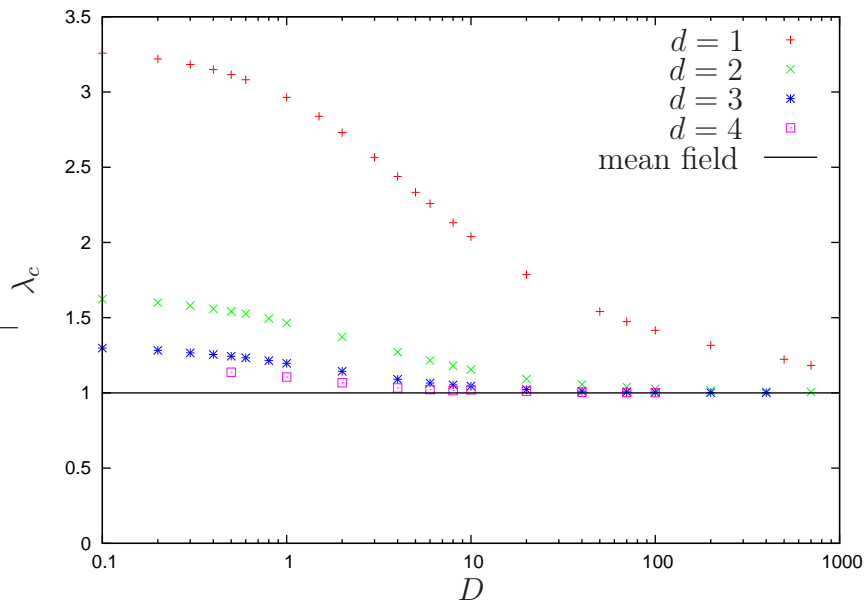
Figure 4.4.: Critical creation rate λ_c derived with numerical simulations for different spatial dimensions compared with mean field prediction. The percolation threshold clearly approaches the mean field value with increasing diffusion rate D. Error-bars have been omitted as they are not visible in this half-logarithmic plot.

this important property and in turn can not give the correct result.

However, with increasing diffusive mixing D, newly created particles spread farther away from their origin before the next creation process occurs. This decreases the number of neighbouring particles and in turn less creation processes will fail. Therefore the effective creation rate approaches the value of λ with increasing diffusion rate. In the limit of infinite diffusion the effective creation rate becomes equal to λ and the mean field result becomes valid.

A second result is that for low diffusion rates the increase of the critical creation rate slows down. This happens when the diffusion constant D becomes comparable to the intrinsic diffusion caused by subsequent creation and annihilation processes.

4.4. Scaling exponents

In the following subsection we will investigate the scaling behaviour of the diffusive contact process in order to verify the field theoretic proposal that
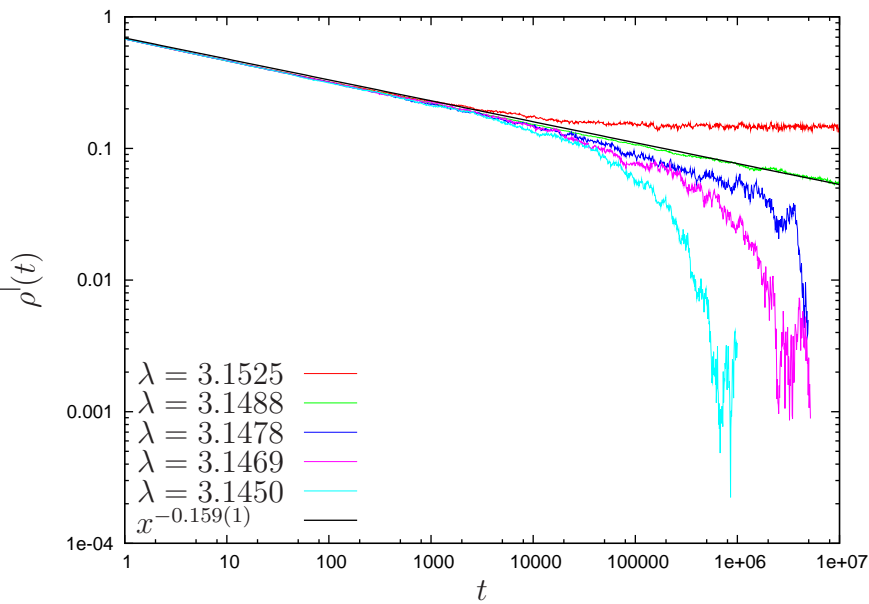
Figure 4.5.: Average particle density as a function of time and creation rate λ. Fitting a power law (black line) to the critical line yields an estimate for the exponent δ. (Simulation parameters: dimension $d = 1$, diffusion constant $D = 0.4$)

the introduction of diffusion does not change the directed percolation scaling exponents.

4.4.1. Decay of density at criticality - exponent δ

Corresponding to section 2.1 the particle density ρ should decay as

$$\langle \rho(t) \rangle \sim t^{-\delta} \tag{4.1}$$

at criticality. Hence to obtain an estimate for δ we fit a power law to the critical density-time curves. An example of this procedure is shown in figure 4.5 where the black line represents the fitted power law.

The estimates for exponent δ obtained using this method are shown in figure 4.6. We see from the plot that in general the exponent is independent from the diffusion rate. The increase of δ in the large diffusion regime for $d = 2$ is mainly caused by the previous explained finite size effects which destroy the power law behaviour. Moreover finite size effects enhance the error estimates.

However, despite of the deviations show these results strong evidence that
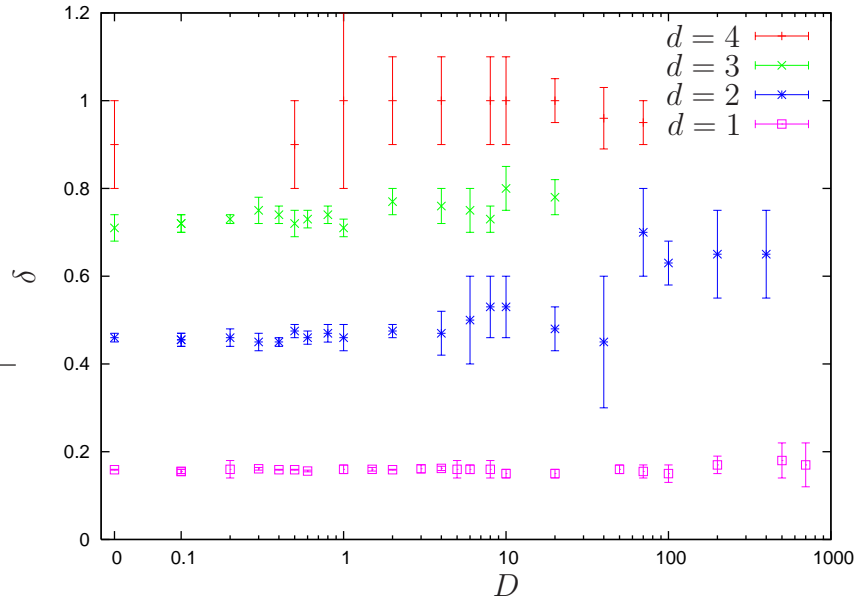
Figure 4.6.: Estimates for scaling exponent δ as a function of the diffusion constant D for various spatial dimensions d. The graph shows that there is no relation between δ and the diffusion rate D. The increase of the exponent for $d = 2$ is mainly caused by finite size effects. The error was estimated by fitting different intervals of the particle density curves.

Table 4.3.: Numerical estimates of scaling exponent δ averaged over the diffusion rate compared to the field theoretic predictions.

dimension	1	2	3	4
δ (Monte Carlo)	0.1598(65)	0.510(78)	0.743(25)	0.971(40)
δ (field theory)	0.25	0.5	0.75	1

the exponent δ does not depend on the value of the diffusion rate. It is therefore sensible to calculate the diffusion average of exponent δ and compare it with the field theoretic result. The averages are presented in table 4.3. These values compare very well to the field theoretic prediction and as well to the estimates given in [7, 14, 6].

4.4.2. Temporal correlation scale - Exponent $\nu_\parallel$

To derive the exponent $\nu_\parallel$ which describes the scaling behaviour of temporal correlation we use the scaling property

$$\langle \rho(t, \lambda) \rangle \sim t^{-\delta} \rho \left(1, t^{1/\nu_\parallel} |\lambda_c - \lambda| \right) \tag{4.2}$$

of the particle density which can be derived by respecting the scale invariant behaviour under transformation (2.15) which was introduced in section 2.

According to this relation every sub- and super-critical curve should collapse on a single sub- and super-critical line if we plot $t^\delta \rho(t)$ versus $t |\lambda_c - \lambda|^{\nu_\parallel}$ when the exponent $\nu_\parallel$ has the correct value. Therefore this exponent can be measured by tuning its value until the curves in such a plot collapse.

An example of this procedure is shown in figure 4.7 where all curves clearly collapse as supposed. Although the accuracy of this method depends on the precision of the previous measured values of λ_c and δ it leads to much better results than calculating the exponent $\nu_\parallel$ from β which would be another way to derive it. (see equations (2.6) and (2.15)).

The results are plotted in figure 4.8. For this measurement the errors bars tend to be very big which is not caused by the used method. Indeed the big measurement errors are again caused by finite size effects which effect that not all curves collapse for the same $\nu_\parallel$. Therefor the error of the measurement increases.

However, the obtained estimates for exponent $\nu_\parallel$ show now relation to the diffusion rate. Therefore we can safely state, that our simulations show that this exponent is also independent from diffusion. Hence the Monte Carlo simulations again confirm the field theoretic proposal.

Calculating the averages of the measured exponents we obtained the values presented in table 4.4. Comparison with field theory shows an increasing devia-
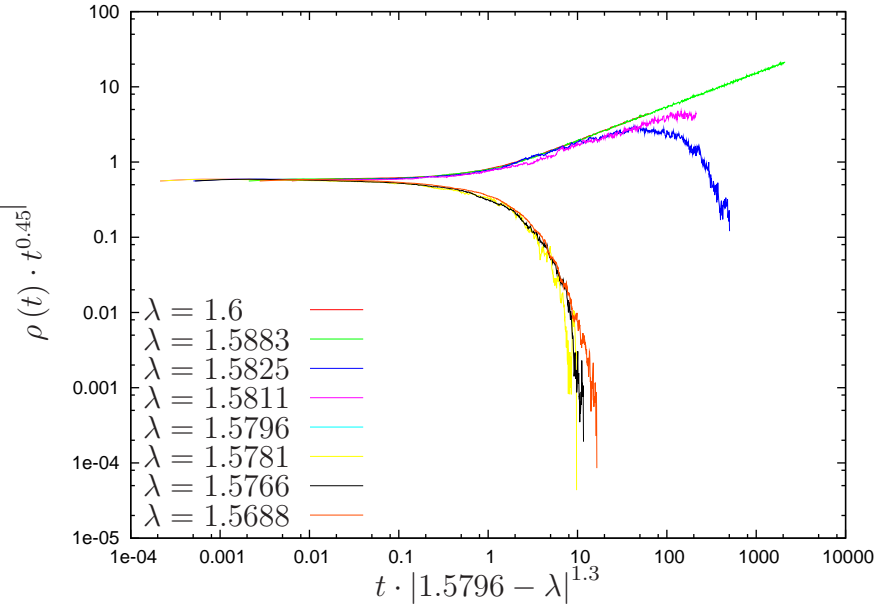
Figure 4.7.: Collapsing density-time curves in order to obtain exponent $\nu_\parallel$. We used the estimate $\delta = 0.45$ obtained previously to scale the density. The graph for $\lambda = 1.5825$ (blue line) is super-critical but shows finite size effects. The collapse yields $\nu_\parallel = 1.3$. (Fixed simulation parameters: dimension $d = 2$, diffusion rate $D = 0.3$)

Table 4.4.: Numerical estimates of scaling exponent $\nu_\parallel$ averaged over diffusion rate compared to field theoretic result.

dimension	1	2	3	4
$\nu_\parallel$ (Monte Carlo)	1.76(15)	1.241(75)	1.04(10)	1.00(14)
$\nu_\parallel$ (field theory)	1.25	1.17	1.08	1

4. Monte Carlo simulation
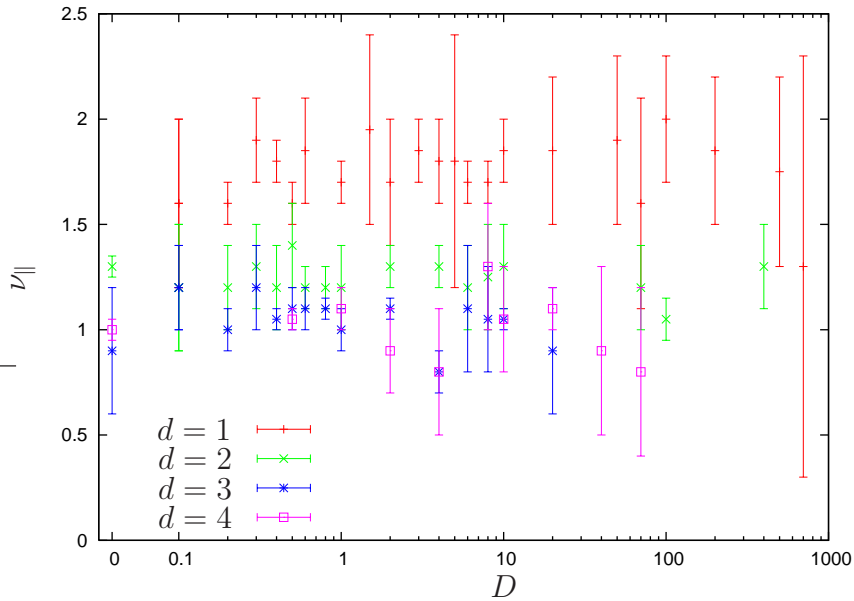
Figure 4.8.: Scaling exponent $\nu_\parallel$ as function of diffusion rate D for spatial dimension $d = 1, 2, 3, 4$. The estimates have been obtained by a data collapsing method. The big error bars reflect the strong influence of finite size effects. But a relation between $\nu_\parallel$ and D is not visible.

tion with decreasing dimension. This expresses the increasing influence of loop corrections. A higher order (two loop, three loop) calculation would lead to a better agreement. Comparing the Monte Carlo results with estimates for the non diffusive contact process presented in [7, 14, 6] shows a good coincidence.

4.4.3. Spatial correlation scale - Exponent $\nu_\perp$

To determine the third scaling exponent we make use of the finite size effects. Starting with an initially fully occupied lattice, the spatial correlation length of an critical system increases with each time step where the increase depends on exponent $\nu_\perp$. At some point the correlation length exceeds the systems size and the particle density collapses. The time point, when this happens, clearly depends on the system size. Therefore in finite systems, observables also depend on the size of the system.

In our case the systems consists of $N = L^d$ lattice sites and as L scales like
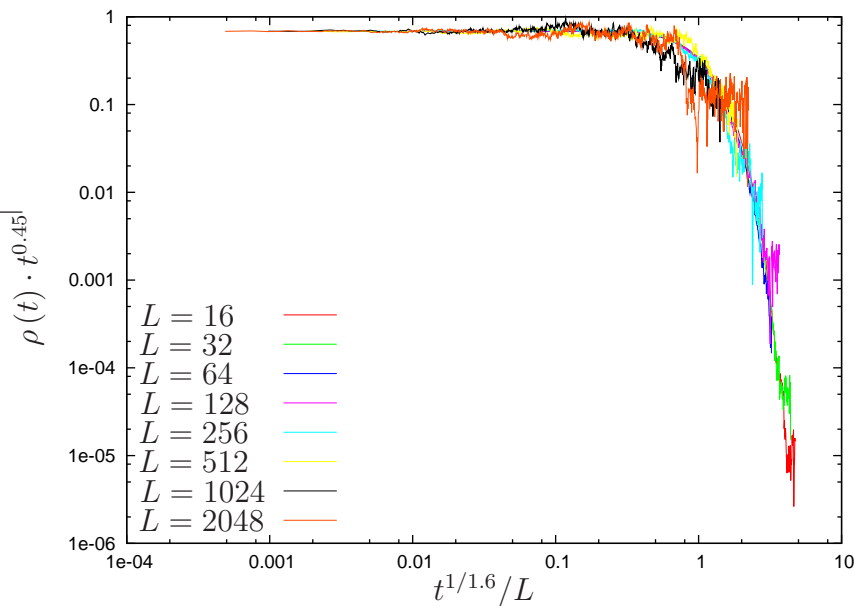
Figure 4.9.: Data collapse of density-time curves of finite size simulations in order to obtain exponent z. To scale the density we used a previous obtained estimate $\delta = 0.45$. The collapse yields $z = 1.6$ for the given set of parameters. (Fixed simulation parameters: spatial dimension $d = 1$, diffusion rate $D = 0$ and creation rate $\lambda = \lambda_c = 3.298$.)

a length we have

$$\langle \rho(t, \Delta, L) \rangle \sim t^{-\delta} \rho \left(1, t^{1/\nu_\parallel} \left(\lambda_c - \lambda \right), \frac{L}{t^{1/z}} \right) \tag{4.3}$$

for the density. Now, at the critical point $(\lambda_c - \lambda)$ vanishes and the density curves collapse. In the same manner as in with $\nu_\parallel$ the exponent $z = \nu_\parallel/\nu_\perp$ can be obtained by tuning it to the appropriate value.

An example of this collapsing is shown in figure 4.9 where all curves coincide on one line.

The estimates for exponent z obtained with this procedure are shown in figure 4.10. What we see from this plot, is that basically the exponent z is independent from the diffusion rate. But for large diffusion rates, it decreases. This behaviour is related to the fact, that the high diffusion rates lead to diffusion length scales which were larger than the system sizes and therefore overrule the increasing (infinite) correlation lengths caused by simulating at the critical point. An increase of the used system sizes would account for this

4. Monte Carlo simulation
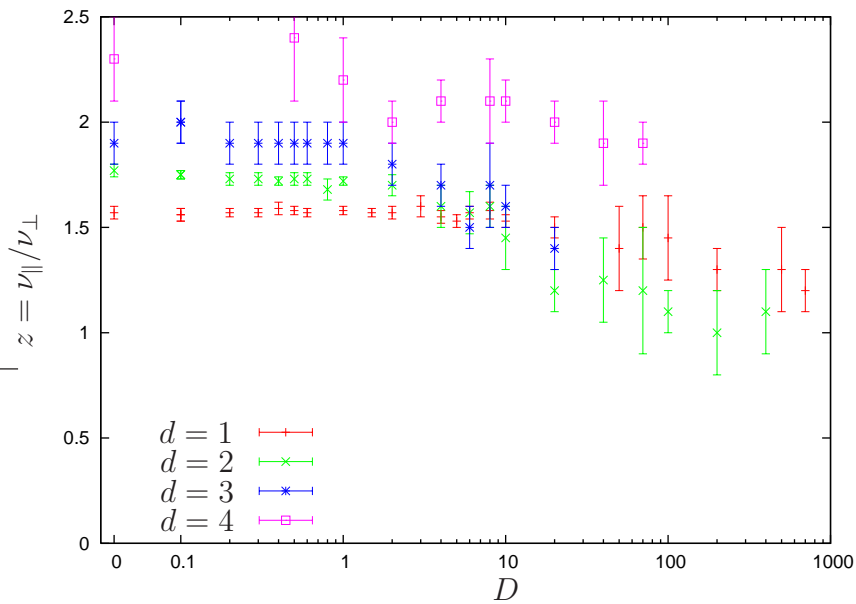
Figure 4.10.: Estimates for scaling exponent $z = \nu_\parallel / \nu_\perp$ as a function of diffusion rate D for spatial dimension $d = 1, 2, 3, 4$. The values have been obtained using the data collapse method described in the text. For large diffusion constants D the diffusion induced mixing suppresses the development of spatial correlations as the systems have a finite size. Hence exponent z decreases.

Table 4.5.: Estimates for scaling exponent $\nu_\perp$ averaged over diffusion rates compared with field theoretic proposal.

dimension	1	2	3	4
$\nu_\perp$ (Monte Carlo)	1.121(98)	0.717(45)	0.544(53)	0.434(64)
$\nu_\perp$ (field theory)	0.688	0.625	0.563	0.5

issue. Unfortunately due to the limited computing power it was not possible to further increase the used system sizes. Hence we exclude the affected data points from further evaluation.

Using relation $z = \nu_\parallel / \nu_\perp$ we derive the spatial scaling exponent $\nu_\perp$ using the values obtained for z and $\nu_\parallel$. Averaging them over the different diffusion rates yields the results presented in table 4.5. Again the deviation of the field theoretic predictions increases with decreasing spatial dimension d due to the one loop precision of the results. Again the Monte Carlo results compare well to previous non diffusive contact process results presented in [7, 14, 6].
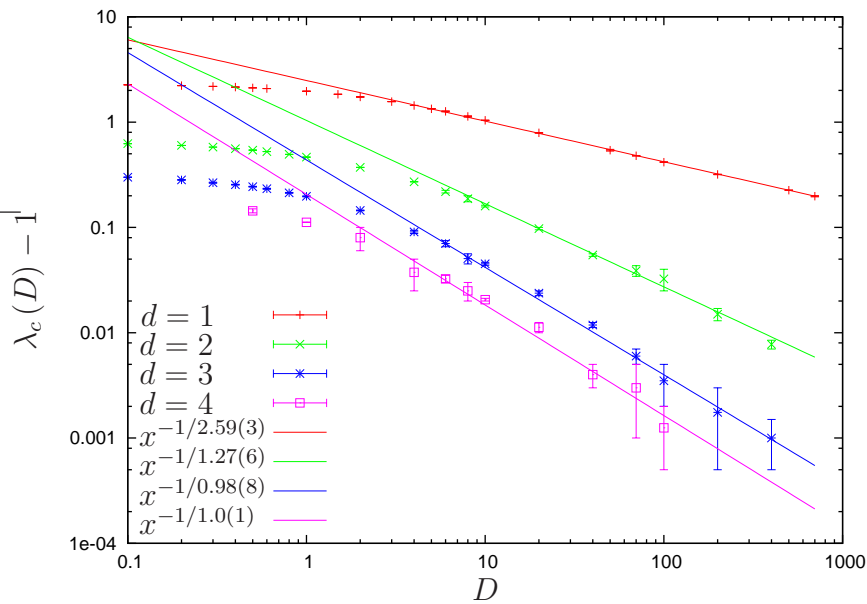
Figure 4.11.: Log-Log plot of $\lambda_c(D)-1$ derived from Monte-Carlo simulations in different spatial dimensions. For large diffusion rates the data points obviously follow a power law. The straight lines are power laws fitted to the large D part of the numerical data.

4.4.4. Crossover behaviour

Derived all scaling exponents, the last task is to focus on the crossover from the low diffusion, directed percolation regime to the high diffusion, mean field behaviour. According to (3.141) we expect

$$\lambda_c - 1 \sim D^{-1/\phi} \tag{4.4}$$

for large diffusion rates D. Therefore we take the data already presented in figure 4.4 and plot $\lambda_c - 1$ against D in a double-logarithmic manner as shown in figure 4.11.

In such a double logarithmic plot, straight lines over at least two decades indicate a power law behaviour, which is clearly the case for our data points in the large diffusion rate regime. The deviation from power law for small diffusion constants is not surprising, as the intrinsic diffusion becomes more important than the explicit diffusion process in this parameter region. In order to derive the crossover exponent ϕ we fit a power law at each curve which is also shown in figure 4.11.

Table 4.6.: Estimates of the cross-over exponent ϕ for spatial dimension $d = 1, 2, 3, 4$ derived from Monte Carlo simulations compared to field theoretic result.

dimension	1	2	3	4
ϕ (Monte Carlo)	2.59(3)	1.27(6)	0.98(8)	1.0(1)
ϕ (field theory)	3	1 + logarithmic corrections	1	1

The obtained exponents are collected in table 4.6. Comparison with field theoretic predictions shows a good agreement even for low spatial dimension. This is related to the fact that the cross-over behaviour is related to the d-dimensional random walk behaviour.

4.5. Numeric Solution of loop correction

So far we verified the field theoretic predictions (3.140) in the large diffusion regime. However for small diffusion rates, analytical solution of (3.139) is easy. Hence we tried to numerically integrate this relation using Mathematica®.

The results of this integration are presented in figure 4.12 and compared with the values obtained from Monte Carlo simulations. In the large diffusion regime the agreement is very well and the numeric integration clearly resembles the Monte Carlo estimates. Unfortunately with decreasing diffusion rate D the suffers from numerical instabilities (divergences) which render the results in this region unusable. Hence we shall state that a numerical integration of (3.138) does not yield improvements over analytical results in this case.

Despite this backstroke the plot shows that for spatial dimension $d = 1$ the numerical integration becomes almost exact over at least two decades and does not show the divergent behaviour as in spatial dimensions $d > 2$. This behaviour is very surprising and has its origin in the behaviour of the d-dimensional random walk.
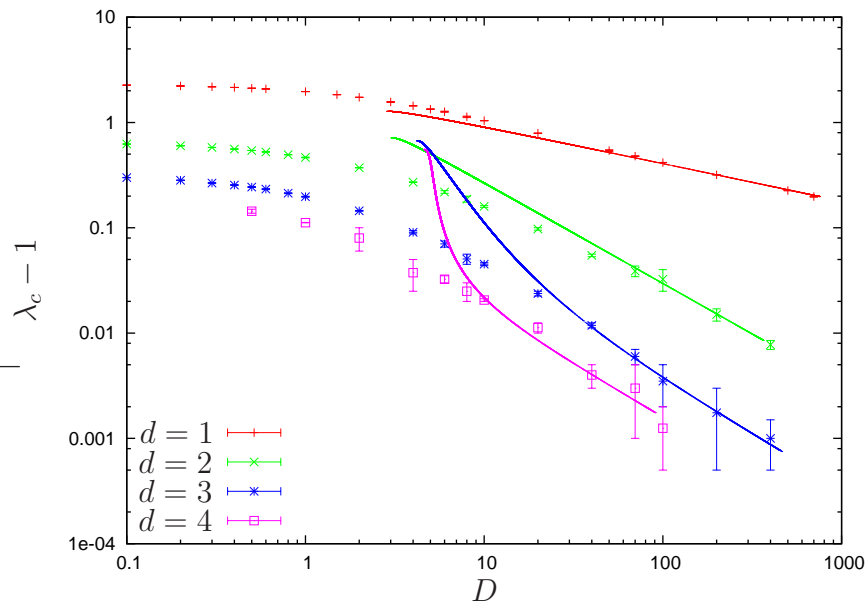
Figure 4.12.: Monte Carlo estimates for critical percolation threshold λ_c (points) compared to numerical integration of (3.138) (solid lines). For large diffusion rates D the agreement is good but since the iteration becomes unstable for small diffusion constants, this region is also not accessible by this approach.

4. Monte Carlo simulation

5. Concluding remarks

Motivated by a previous work of Dantas et al. [2] we considered the diffusive extension of the contact process in this work. We have studied the influence of diffusion of particles on universal properties of the contact process using field theoretic calculations and verified them using Monte Carlo simulations.

Naturally, introduction of diffusion does not change geometric properties of a model. Therefore one expects that scaling exponents are not affected by introducing a short range diffusion process. Using dimensional regularisation and multiplicative renormalisation of the field theoretic model we confirmed this. Furthermore the field theoretic treatment predicted that the scaling exponents are independent from the diffusion rate and equal to the directed percolation exponents. Therefore the diffusive contact process also belongs into the directed percolation universality class of non-equilibrium absorbing state phase transitions.

Further on the field theoretic calculations yield, that the critical control parameter λ_c depends on the diffusion constant and approaches the mean field value as a power law for large diffusion rates (3.140). The exponent ϕ of this power law is governed by the properties of the d-dimensional random walk and therefore strongly depends on the spatial dimension if $d < 2$. Indeed for higher space dimensions ϕ becomes a constant. This result confirms a previous work by Konno [8] but was derived in a much simpler way.

To verify the predictions of the field theoretic model we used numeric simulations. Hence we simulated the diffusive contact process for many different system parameters using a Monte Carlo based algorithm. Analysis of the numerical data yielded estimates for exponents and critical creation rates. The results compared well with the analytical model. Moreover the good agreement shows evidence that field theory is a powerful tool for studying such non-equilibrium absorbing state phase transitions.

Finally we compared the Monte Carlo results with a numeric solution of

5. Concluding remarks

(3.139) were we showed that in this case the analytical calculation can not improved by numerical integration. Despite that we observed that in one spatial dimension the one loop correction when evaluated numerically is in better agreement with the Monte Carlo results than the results in three or four dimensions. This is surprising as one expects loop corrections to be more relevant in low dimensional systems. A further investigation of this issue may be sensible.

A. Introduction on field mathematics

In this appendix we would like to give a very short introduction into the formalism used for fields, functional integrals and functional derivatives in this work.

The fields we use in our calculations are basically variables which are labelled with continuous indexes. For instance we can define a continuous density field from a density defined on a lattice in limit of a zero lattice constant. Considering a two-dimensional lattice with integer indexes i and j we introduce a density ρ_{ij} at each lattice site. Let Δ be the lattice constant - this is the spacing between two nearest neighbouring sites. We can now define a space and time coordinate setting

$$x = i \cdot \Delta, \quad t = j \cdot \Delta \tag{A.1}$$

which become continuous in the limit $\Delta \to 0$:

$$\rho(x, t) = \lim_{\Delta \to 0} \rho_{ij}. \tag{A.2}$$

Using this definition it is now possible to define a functional integral as a product of integrals at each lattice point. We find

$$\int D\rho = \lim_{\Delta \to 0} \prod_{i,j}^{\infty} \int d\rho_{ij} \tag{A.3}$$

for a functional integral. Here we absorbed the normalisation factor into the integral measure. Moreover a functional derivative (variation) can be defined as the result of

$$\frac{\delta}{\delta \rho(x, t)} = \lim_{\Delta \to 0} \frac{\delta}{\delta \rho_{ij}}. \tag{A.4}$$

A. Introduction on field mathematics

Finally it is also possible to integrate the space and time coordinates. This corresponds to a sum of the fields over all space time points:

$$\int dx \int dt \rho(x, t) = \lim_{\Delta \to 0} \sum_{i=-\infty}^{\infty} \sum_{j=-\infty}^{\infty} \rho_{ij} \qquad \text{(A.5)}$$

B. Data

The Compact-Disc attached to the back cover of this thesis contains a copy of the data created during working out the thesis. The directory structure is as follows:

/data Exponents derived from Monte-Carlo simulations.

/data/critical, /data/finite-size Density-time curves obtained from Monte Carlo simulations split into single files.

/data/matlab Matlab functions used for analysis of numerical data as well as a copy of the matlab workspace.

/mathematica Mathematica notebooks created for field theoretic renormalisation and numerical integration.

/src This directory contains the entire source code of the application used for the Monte Carlo simulations. The simulation is split into a client- and a server-program. While the client application can be used stand alone using command line switches, the server application is responsible for distributing simulation parameters over a network and collecting simulation results from computing clients. Hence client programs have to attach to a running server application in order to do something useful. The server stores its data in a single *sqlite*[1]-database file. In order to compile it a recent libsqlite3 must be available. To compile one of the programs, copy the directory to your hard-disc, dive into the directory with a shell and type

```
make cp-client-<dimension>-<lattice-length>
make cp-data-server
```

---

[1]http:\\www.sqlite.org

where $<$*dimension*$>$ and $<$*lattice-length*$>$ have to be replaced by the desired numbers.

/thesis Latex source code of diploma thesis

List of Figures

64

List of Figures

List of Tables

List of Tables

Bibliography

[1] S. R. Broadbent and J. M. Hammersley. *Proc. Camb, phil. Soc.*, 53:629, 1957.

[2] W. G. Dantas, M. J. de Oliveira, and J. F. Stilck. Revisiting the one-dimensional diffusive contact process. *J. Stat. Mech.*, page P08009, 2007.

[3] T. E. Harris. Contact interactions on a lattice. *Annals of Probability*, 2 (6):969, 1957.

[4] H. Hinrichsen. Non-equilibrium critical phenomena and phase transitions into absorbing states. *Adv. Phys.*, 49:815, 2000. [cond-mat/0001070].

[5] H. K. Janssen. On the non-equilibrium phase transition in reaction-diffusion systems with an absorbing stationary state. *Z. Phys. B*, 42:151, 1981.

[6] I. Jensen. Critical behavior of the three-dimensional contact process. *Phys. Rev. A*, 45(2):R563, Jan 1992. doi: 10.1103/PhysRevA.45.R563.

[7] I. Jensen. Low-density series expansions for directed percolation: I. a new efficient algorithm with applications to the square lattice. *J. Phys A.*, 32: 5233, 1999.

[8] N. Konno. Asymptotic behavior of basic contact process with rapid stirring. *J. Theo. Prob.*, 8:833, 1995.

[9] A. M. and H. Hinrichsen. Crossover from directed percolation to mean field behavior in the diffusive contact process. *J. Stat. Mech.: Theor. Exp.*, page P04024, 2008. doi: 10.1088/1742-5468/2008/04/P04024.

[10] M. Maggiore. *A Modern Introduction to Quantum Field Theory.* Oxford University Press, Oxford, 2005.

Bibliography

[11] M. E. Peskin and D. V. Schroeder. *An Introduction to Quantum Field Theory.* Addison-Wesley, Reading, MA, 1995.

[12] L. H. Ryder. *Quantum field theory.* Cambridge University Press, Cambridge, 1996.

[13] U. C. Täuber. Field theory approaches to nonequilibrium dynamics. *Lect. Notes Phys.*, 716:295, 2007. doi: 10.1007/3-540-69684-9_7.

[14] C. A. Voigt and R. M. Ziff. Epidemic analysis of the second-order transition in the ziff-gulari-barshad surface-reaction model. *Phys. Rev. E*, 56(6): R6241, Dec 1997. doi: 10.1103/PhysRevE.56.R6241.

[15] K. G. Wilson. Renormalization group and critical phenomena. i. renormalization group and the kadanoff scaling picture. *Phys. Rev. B*, 4(9): 3174, Nov 1971. doi: 10.1103/PhysRevB.4.3174.

[16] R. M. Ziff. Four-tap shift-register-sequence random-number generators. *Computers in Physics*, 12(4):385, July 1998. doi: 10.1063/1.168692.

Acknowledgements

The author wants to thank all persons who supported him during the university education and diploma thesis. Special thanks go to

- Prof. Dr. Haye Hinrichsen for the opportunity to write my thesis in his group.

- Alexander Schenkel for various field theory related discussions.

- Anja Englert for carefully reading of this work.

Erklärung

Hiermit erkläre ich, dass ich die vorliegende Arbeit selbständig verfasst und
keine anderen als die angegebenen Hilfsmittel verwendet habe.

Würzburg den 8. Juli 2008 Andreas Messer